

Cosmological simulations of galaxy formation

Mark Vogelsberger¹*, Federico Marinacci¹, Paul Torrey¹, Ewald Puchwein¹

Abstract | Over recent decades, cosmological simulations of galaxy formation have been instrumental in advancing our understanding of structure and galaxy formation in the Universe. These simulations follow the nonlinear evolution of galaxies, modelling a variety of physical processes over an enormous range of time and length scales. A better understanding of the relevant physical processes, improved numerical methods and increased computing power have led to simulations that can reproduce a large number of the observed galaxy properties. Modern simulations model dark matter, dark energy and ordinary matter in an expanding space-time starting from well-defined initial conditions. The modelling of ordinary matter is most challenging due to the large array of physical processes affecting this component. Cosmological simulations have also proven useful to study alternative cosmological models and their impact on the galaxy population. This Technical Review presents a concise overview of the methodology of cosmological simulations of galaxy formation and their different applications.

Modern astronomical surveys provide enormous amounts of observational data that confront our theories of structure and galaxy formation. Interpreting these observations requires accurate theoretical predictions. However, galaxy formation is a challenging problem due to its intrinsic multiscale and multiphysics character. Cosmological computer simulations are, hence, the method of choice for tackling these complexities when studying the properties, growth and evolution of galaxies. These simulations are important to understand the detailed workings of structure and galaxy formation. Dark matter builds the backbone for structure formation and is therefore a key ingredient of these simulations. In addition, dark energy is responsible for the accelerated expansion of the Universe and must also be considered. Despite the fact that the nature of dark matter and dark energy are not known, simulations can make detailed and reliable predictions for these dark components based on their general characteristics. Ordinary matter, such as stars and gas, contribute only about five percent to the energy budget of the Universe. Nevertheless, simulating this matter component is essential to study galaxies, but, unfortunately, it is also the most challenging aspect of galaxy formation. Recent simulations follow the formation of individual galaxies and galaxy populations from well-defined initial conditions and yield realistic galaxy properties¹. Examples of visual representations of the predictions of some of these simulations are shown in FIG. 1. At the heart of these simulations are detailed galaxy formation models. Among others, these models describe the cooling of gas, the

formation of stars, and the energy and momentum injection caused by supermassive black holes and massive stars². Nowadays, simulations also model the impact of radiation fields, relativistic particles and magnetic fields, leading to an increasingly complex description of the galactic ecosystem and the detailed evolution of galaxies in the cosmological context. Galaxy formation simulations have also become important for cosmological studies since they can, for example, explore the impact of alternative cosmological models on the galaxy population. Cosmological simulations of galaxy formation therefore provide important insights into a wide range of problems in astrophysics and cosmology. The most important components of cosmological galaxy formation simulations are discussed in this Technical Review. A schematic overview of the different ingredients of cosmological simulations is presented in FIG. 2.

Cosmological framework

Cosmological simulations of galaxy formation are performed within a cosmological model and start from specific initial conditions. Both of these ingredients are now believed to be known to high precision.

Cosmological model

Various observations have revealed that our Universe is geometrically flat and dominated by dark matter and dark energy accounting for about ~95% of the energy density. Standard model particles make up for the remaining ~5% and are collectively referred to as baryons. The leading model for structure formation

¹Department of Physics,
Kavli Institute for
Astrophysics and Space
Research, Massachusetts
Institute of Technology,
Cambridge, MA, USA.

²Department of Physics and
Astronomy, University of
Bologna, Bologna, Italy.

³Department of Astronomy,
University of Florida,
Gainesville, FL, USA.

⁴Leibniz-Institut für
Astrophysik Potsdam,
Potsdam, Germany.

*e-mail: mvogelsb@mit.edu
<https://doi.org/10.1038/s42254-019-0127-2>

Key points

- The formation of structures and galaxies in the Universe, which consists of ordinary matter, dark energy and dark matter, involves various physical processes such as gravity, gas cooling, star formation, supernova feedback, supermassive black hole feedback, stellar evolution, radiation, magnetic fields, cosmic rays and more.
- Cosmological simulations allow detailed studies of the formation and evolution of structures and galaxies in the cosmos, starting from smooth initial conditions constrained through observations of the cosmic microwave background, yielding detailed predictions of the galaxy population at different epochs of the Universe.
- The dark matter component is typically numerically modelled through the *N*-body approach. Here, the dark matter phase-space distribution is sampled by an ensemble of phase-space sampling points, resulting in a Monte Carlo scheme, to follow its dynamics, which are governed by the collisionless Boltzmann equation.
- The gas content of the baryonic matter component is, in its simplest form, described through the Euler equations, discretized with Eulerian, Lagrangian or arbitrary Lagrangian–Eulerian schemes, coupled to other physical processes such as gravity, cooling processes, feedback processes and star formation.
- Alternative forms of dark matter, dark energy and gravity can also be explored through suitable modified simulation methods to test and constrain such theories in the context of structure and galaxy formation, by comparing to observational data such as galaxy surveys, leading to important insights into the overall cosmological framework of structure formation and cosmological parameters.

assumes that dark matter is cold, with negligible random motions when decoupled from other matter, and collisionless. Dark energy is represented by a cosmological constant Λ , which drives the accelerated expansion of the Universe. These make the Λ CDM (cold dark matter) model, which builds the framework for galaxy formation. Measurements of the cosmic microwave background combined with other observations, such as the distance-redshift relation from type Ia supernovae, abundances of galaxy clusters and galaxy clustering, constrain the fundamental parameters of the Λ CDM model³.

Initial conditions

Initial conditions for cosmological simulations specify the perturbations imposed on top of a homogeneous expanding background. The background model is generally taken to be a spatially flat Friedmann–Lemaître–Robertson–Walker space-time with a defined composition of dark matter, dark energy and baryons. Inflation predicts Gaussian perturbations, where the joint probability distribution of density fluctuations is a multi-dimensional Gaussian completely specified by its matter power spectrum $P(|k|)$, where k is the wavenumber. The post-recombination density field is the linear convolution of the primordial fluctuation field as predicted by inflation with a transfer function $T(k)$ (REFS^{4–7}).

Therefore, the power spectrum used to initialize simulations generally takes the form $P(k) = Ak^n|T(k)|^2$ with $n \approx 1$ and amplitude A . Once the linear density fluctuation field has been specified at some initial time, typically at redshift $z \sim 100$, dark matter particle positions and velocities are assigned along with baryon density, velocity and temperature fields. The standard approach for dark matter is to displace simulation particles from a uniform Cartesian lattice or glass-like^{8,9} particle configuration using a linear theory approximation¹⁰ or low-order perturbation theory^{11–14} (BOX 1). A gravitational glass is made by advancing particles from random

Friedmann–Lemaître–Robertson–Walker space-time

A metric that is an exact solution of Einstein's field equations of general relativity describing a homogeneous, isotropic, expanding universe.

Comoving coordinates
Spatial coordinates within an isotropic and uniformly expanding universe, where the overall expansion is divided out.

Method of characteristics
A technique for solving partial differential equations based on finding curves along which the original partial differential equation becomes an ordinary differential equation.

positions using the opposite sign of gravity until they freeze in comoving coordinates. Baryon positions and velocities are set in a similar way, and the baryon temperature is often roughly initialized to the redshift-dependent microwave background temperature. Two types of initial conditions are commonly used: uniformly sampled periodic large volumes or zoom initial conditions, where a low-resolution background realization of the density fields surrounds a high-resolution region of interest. The computational cost of these zoom simulations increases with the mass of the object that is studied for a given mass resolution. Zoom simulations of dwarf galaxies are therefore computationally less expensive than zoom simulations of large galaxy clusters given the larger number of simulation resolution elements of the latter. Some simulations also use constrained initial conditions to mimic, for example, the local Universe, such as nearby dark matter overdensities^{15,16}.

Simulating dark matter

Dark matter builds the backbone for the formation of galaxies, which are expected to emerge at the centres of dark matter overdensities, so-called halos. The continuum limit of non-interacting dark matter particles is described by the collisionless Boltzmann equation coupled to Poisson's equation (BOX 1). This pair of equations has to be solved in an expanding background universe described by the Friedmann equations, which are derived from the field equations of general relativity. Most cosmological simulations use Newtonian rather than relativistic gravity, which provides a good approximation since linear structure growth is identical in the matter-dominated regime in the two theories, and nonlinear large-scale structure induces velocities far below the speed of light. Cosmological simulations are also typically performed with periodic boundary conditions to mimic the large-scale homogeneity and isotropy of the matter distribution of the Universe, that is, the cosmological principle.

Numerical techniques

The high dimensionality of the collisionless Boltzmann equation prohibits efficient numerical solution methods based on standard discretization techniques for partial differential equations. Therefore, over recent decades, other numerical techniques have been developed to solve this problem more efficiently. An overview of some selected simulation codes and the employed dark matter simulation techniques is presented in TABLE 1.

The *N*-body method. *N*-body methods are often used to follow the collisionless dynamics of dark matter, where the phase-space density is sampled by an ensemble of *N* phase-space points $\mathbf{r}_i, \dot{\mathbf{r}}_i, i = 1 \dots N$ with masses m_i . The conservation of the phase-space density f along the particle flow implies that the masses m_i remain unchanged along each trajectory. *N*-body methods therefore solve the collisionless Boltzmann equation by the method of characteristics. Alternatively, this method can also be interpreted as a Monte Carlo technique, since any initial sample of *N* phase-space points drawn from the same phase-space density at time $t = 0$

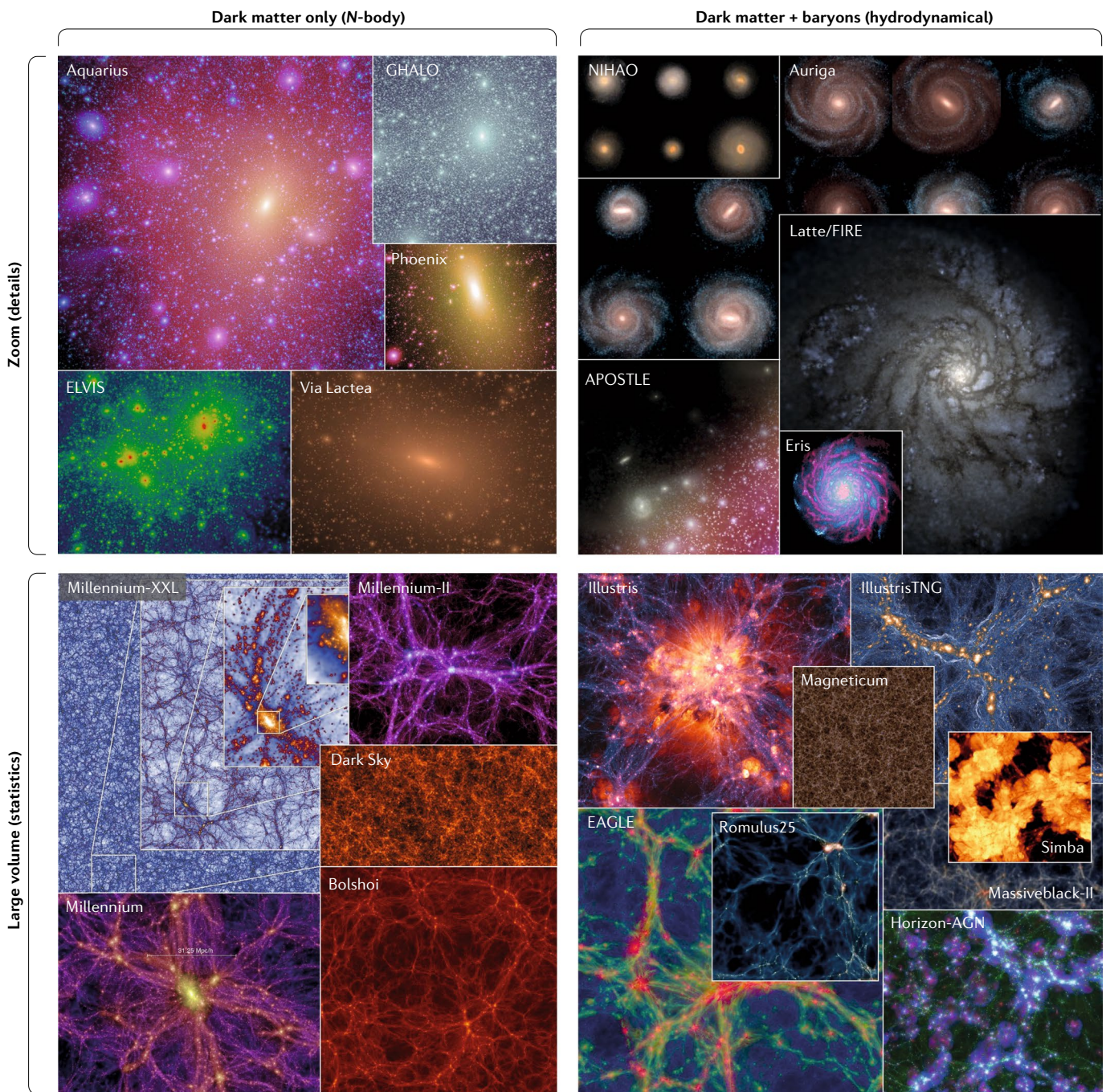


Fig. 1 | Visual representations of some selected structure and galaxy formation simulations. The simulations are divided into large-volume simulations that provide statistical samples of galaxies and zoom simulations that resolve smaller scales in more detail. They are also divided in dark matter-only simulations, such as *N*-body simulations, and dark matter plus baryons simulations, such as hydrodynamical simulations. Dark matter-only simulations have now converged on a wide range of predictions for the large-scale clustering of dark matter and the dark matter distribution within gravitationally bound dark matter halos. Recent hydrodynamical simulations reproduce galaxy populations that agree remarkably well with observational data. However, many detailed predictions of these simulations are still sensitive to the underlying implementation of baryonic physics. Image of the Aquarius project courtesy of Volker Springel, Max-Planck-Institute. GHALO is reproduced with permission from REF.⁴⁰⁸, Oxford University Press. Phoenix is reproduced with permission from REF.⁹², Oxford University Press. ELVIS is adapted with permission of Shea Garrison Kimmel from REF.⁴⁰⁹. Via Lactea image courtesy of Dr Joachim Stadel, University of Zurich. NIHAO is adapted with permission from REF.¹¹², Oxford University Press.

Auriga image courtesy © MPA/Virgo consortium. APOSTLE image courtesy Till Sawala, University of Helsinki. Latte/FIRE image adapted with permission from REF¹³⁵, Oxford University Press. Eris image courtesy of Lucio Mayer and Simone Callegari, University of Zurich. Millennium image courtesy of Volker Springel, Max-Planck-Institute; Millennium-XXL courtesy © Millennium simulation/MPA/Virgo consortium; Millennium-II image courtesy of Mike Boylan-Kolchin/Millennium-II Simulation. Dark Sky is adapted from REF.⁴², Skillman, S. W. et al. Dark sky simulations: early data release. *arXiv e-prints* (2014). Bolshoi image courtesy of S. Gottlöber; IDL: <https://www.cosmosim.org/cms/images-and-movies/>. Illustris image courtesy of Illustris Collaboration; IllustrisTNG image courtesy of D. Nelson, TNG Collaboration. Magneticum image adapted with permission from Dolag (2015)¹⁰. Simba is adapted with permission from REF¹⁷¹, Oxford University Press. Massiveblack-II is reproduced from REF.⁴¹¹, Oxford University Press. Romulus25 image courtesy of Tom Quinn, University of Washington and Michael Tremmel, Yale University. EAGLE adapted with permission from REF.¹¹¹, Oxford University Press. Horizon-AGN image courtesy of Christophe Pichon, Horizon Simulation Group, <https://www.horizon-simulation.org/media.html>.

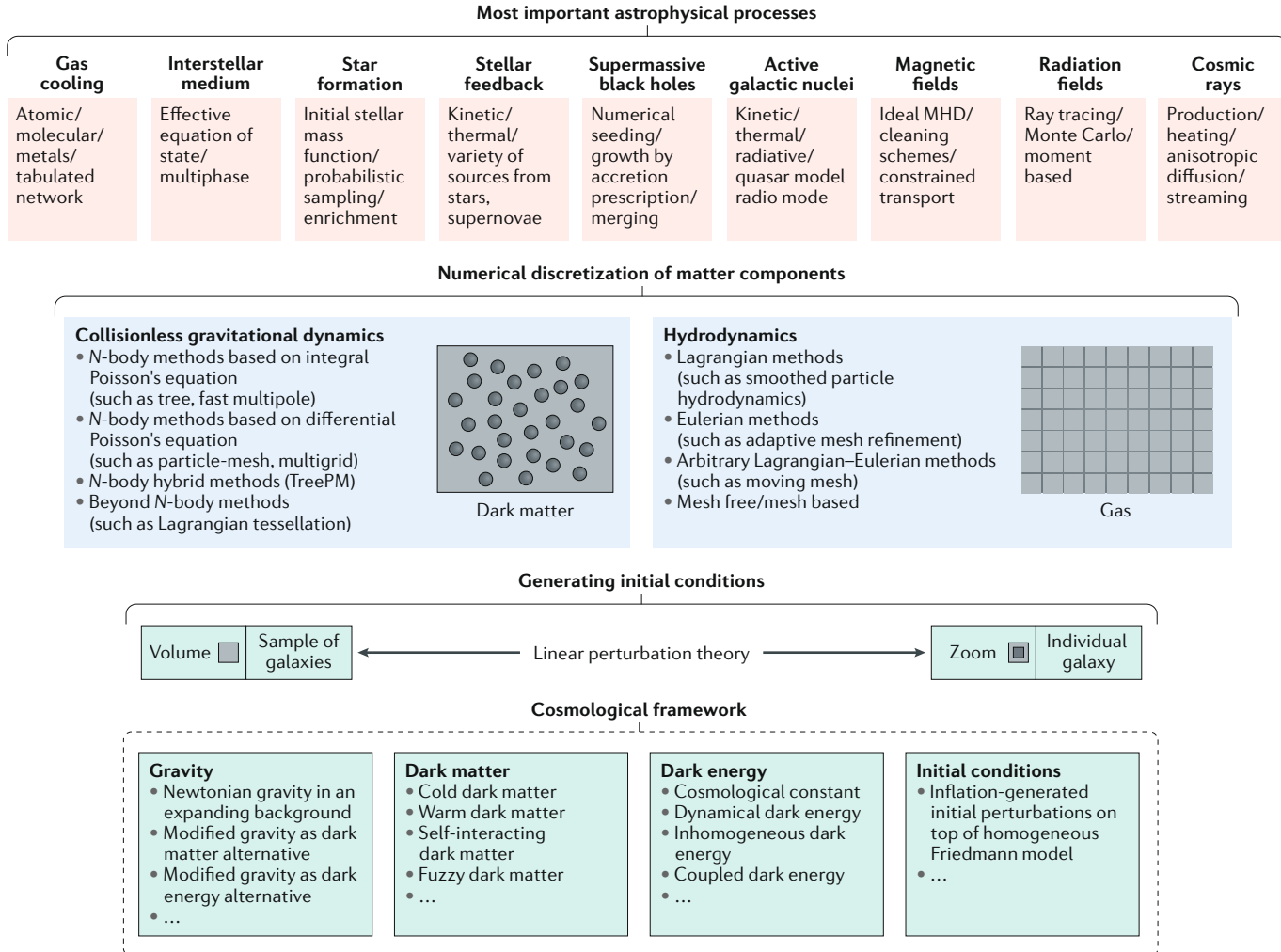


Fig. 2 | Overview of the key ingredients of cosmological simulations. These simulations are performed within a given cosmological framework and start from specific initial conditions. The framework includes physical models for gravity, dark matter, dark energy and the type of initial conditions. Two types of simulations are typically performed: either large-volume simulations or zoom simulations. The evolution equations of the main matter components, dark matter and gas, are discretized using different techniques and evolved forward in time. The dark matter component follows the equations of collisionless gravitational dynamics that are in most cases solved through the N-body method using different techniques to calculate the gravitational forces. The gas component of baryons is described through the equations of hydrodynamics that are solved, for example, with Lagrangian or Eulerian methods. Various astrophysical processes must also be considered to achieve a realistic galaxy population. Many of these are implemented through effective subresolution models. MHD, magnetohydrodynamics; TreePM, tree + particle-mesh.

results in an N -body model for the time evolution of $f(\mathbf{r}, \dot{\mathbf{r}}, t)$. The ensemble of all N particles together represents the coarse-grained phase-space density $\langle f \rangle \approx \sum_i m_i f(\mathbf{r}_i(t), \dot{\mathbf{r}}_i(t))$. The latter represents a typical Monte Carlo estimate that can be applied also to other quantities, such as the configuration space density. This sampling is subject to Poisson noise, and high particle numbers are therefore desirable to reduce noise in these estimates. To avoid unphysical two-body scattering between nearby particles, gravitational interactions are softened on small scales so that the particle collection represents a smoothed density field. A variety of kernel-based smoothing techniques are implemented, and some simulations also implement adaptive softening schemes to reduce the softening length in high-density regions to reach higher spatial force resolution¹⁷.

The main challenge of N -body simulations is to efficiently calculate the gravitational force that governs the motion of the dark matter sample particles. Once the forces have been calculated, the particles are advanced based on symplectic integration schemes commonly implemented through a Leapfrog integrator. Symplectic integrators exactly solve an approximate Hamiltonian such that the numerical time evolution is a canonical map and preserves certain conserved quantities, such as the total angular momentum and the phase-space volume. Cosmological simulations are further confronted with a large dynamic range in timescales; for example, in high-density regions, orders of magnitude smaller time steps are required than in low-density regions. Integration schemes with individual time steps are therefore typically used. The time integration

Box 1 | Initial conditions and modelling

Generating initial conditions

- initial positions

$$\mathbf{x} = \mathbf{q} + D(t)\Psi(\mathbf{q})$$
- initial velocities

$$a(t)\mathbf{x} = a(t)\frac{dD(t)}{dt} \Psi(\mathbf{q}) = a(t)H(t)\frac{d\ln D}{d\ln a}D(t)\Psi(\mathbf{q})$$

Comoving initial positions, \mathbf{x} , are assigned based on the unperturbed particle position, \mathbf{q} , the linear growth factor, $D(t)$ and the scale factor, a , which is related to the initial redshift, $z = 1/a - 1$. The curl-free displacement field Ψ is computed by solving the linearized continuity equation $\nabla \cdot \Psi = -\delta/D(t)$, where δ is the relative density fluctuation and H is the Hubble function.

Modelling dark matter

- collisionless Boltzmann equation

$$\frac{df}{dt} + \mathbf{v} \cdot \frac{\partial f}{\partial \mathbf{r}} - \frac{\partial \Phi}{\partial \mathbf{r}} \frac{\partial f}{\partial \mathbf{v}} = 0$$

- Poisson's equation

$$\nabla^2 \Phi = 4\pi G \int f d\mathbf{v}$$

The collisionless Boltzmann equation describes the evolution of the phase-space density or distribution function of dark matter, $f = f(\mathbf{r}, \mathbf{v}, t)$, with \mathbf{r} , the positions and \mathbf{v} , the velocities, under the influence of the collective gravitational potential, Φ , with G the gravitational constant, given by Poisson's equation. The collisionless Boltzmann equation states the conservation of the local phase-space density; that is Liouville's theorem.

Modelling cosmic gas

- Eulerian formulation

$$\frac{\partial \rho}{\partial t} + \nabla \cdot (\rho \mathbf{v}) = 0$$

$$\frac{\partial \rho \mathbf{v}}{\partial t} + \nabla \cdot (\rho \mathbf{v} \otimes \mathbf{v} + P \mathbf{I}) = 0$$

$$\frac{\partial \rho e}{\partial t} + \nabla \cdot (\rho e + P) \mathbf{v} = 0$$

- Lagrangian formulation

$$\frac{D\rho}{Dt} = -\rho \nabla \cdot \mathbf{v}$$

$$\frac{D\mathbf{v}}{Dt} = -\frac{1}{\rho} \nabla P$$

$$\frac{De}{Dt} = -\frac{1}{\rho} \nabla \cdot P \mathbf{v}$$

- Arbitrary Lagrangian–Eulerian formulation

$$\frac{d}{dt} \int_V \rho dV = - \int_S \rho (\mathbf{v} - \mathbf{w}) \cdot \mathbf{n} dS$$

$$\frac{d}{dt} \int_V \rho \mathbf{v} dV = - \int_S \rho \mathbf{v} (\mathbf{v} - \mathbf{w}) \cdot \mathbf{n} dS - \int_S P \mathbf{n} dS$$

$$\frac{d}{dt} \int_V \rho e dV = - \int_S \rho e (\mathbf{v} - \mathbf{w}) \cdot \mathbf{n} dS - \int_S P \mathbf{v} \cdot \mathbf{n} dS$$

Here, S is the surface (area integrals) and \mathbf{n} is the normal vector on the surface. ρ is the density, and u is the internal energy. Different forms of the hydrodynamical equations. $D/dt \equiv \partial/\partial t + \mathbf{v} \cdot \nabla$ denotes the Lagrangian derivative and $e = u + \mathbf{v}^2/2$ the total energy per unit mass. The equations are closed through $P = (\gamma - 1)\rho u$ with $\gamma = 5/3$. For the arbitrary Lagrangian–Eulerian formulation, the grid moves with velocity \mathbf{w} and cell volumes evolve as $dV/dt = \int_V (\nabla \cdot \mathbf{w}) dV$.

is no longer symplectic in a formal sense when individual short-range time steps are chosen for different particles. Methods to calculate the gravitational forces of the N -body system can roughly be divided into two groups: approaches to accelerate the direct summation problem through approximations or mesh-based methods to calculate the forces. The former approaches aim for efficient numerical solutions of the integral form of Poisson's equation. The latter methods aim for efficient techniques to solve the differential form of Poisson's equation.

- Solving the integral form of Poisson's equation.

Using the integral form of Poisson's equation, $\Phi(\mathbf{r}) = -G \int d\mathbf{r}' \rho(\mathbf{r}') / |\mathbf{r} - \mathbf{r}'|$, where G is the gravitational constant and Φ is the potential, the density can be translated to a discrete direct summation problem with complexity $\mathcal{O}(N^2)$. Solving this problem directly results in the so-called particle-particle scheme, and the earliest simulations used this brute-force approach. The most common method to accelerate the direct summation through approximations is the so-called tree approach¹⁸. Here, contributions to the gravitational potential from distant particles are approximated by the lowest-order terms in a multipole expansion of the mass distribution at a coarse level of the tree reducing the computational cost to $\mathcal{O}(N \log N)$. The approximation used in the tree method is formally obtained by Taylor expanding the force around some expansion centre of the particle group. Often, an octree is implemented in cosmological simulations, where each cubic cell is split into up to eight child cells resulting in a tree-like hierarchy of cubic nodes with the root node containing all particles at its bottom. The particles within each of the tree nodes constitute a well-defined and localized group that build the basis for the tree force calculation. A further improvement to the $\mathcal{O}(N)$ complexity is possible through the use of the fast multipole method, where forces are calculated between two tree nodes rather than between individual particles and nodes. This method is best implemented using a tree structure¹⁹, although the original proposed method was based on a fixed mesh²⁰. Implementing periodic boundary conditions for these direct summation-based schemes typically requires Ewald summation techniques²¹ originally developed for solid-state physics²².

- Solving the differential form of Poisson's equation.

Mesh-based methods aim to solve the differential form of Poisson's equation, $\nabla^2 \Phi(\mathbf{r}) = 4\pi G \rho(\mathbf{r})$, in which ρ is the density. This equation can be solved efficiently through fast Fourier transform-based methods, with Poisson's equation in Fourier space $k^2 \tilde{\Phi}(\mathbf{k}) = -4\pi G \tilde{\rho}(\mathbf{k})$, leading to the so-called particle-mesh method²³. Quantities with tildes are Fourier transformed quantities. To obtain forces, the potential is then differentiated using a finite difference approximation and the forces are interpolated to the particle positions. The calculation of the gravitational forces using a fast Fourier transform has only a $\mathcal{O}(N \log N)$ complexity, where N is the number of mesh cells. The computational cost does not depend

Table 1 | Major galaxy formation simulation codes

Code name	Gravity treatment	Hydrodynamics treatment	Parallelization technique	Code availability	Refs
ART	PM/ML	AMR	Data based	Public	27
RAMSES	PM/ML	AMR	Data based	Public	412
GADGET-2/3	TreePM	SPH	Data based	Public	413
Arepo	TreePM	MMFV	Data based	Public	116
Enzo	PM/MG	AMR	Data based	Public	414
ChaNGa ^a	Tree/FM	SPH	Task based	Public	415–417
GIZMO ^b	TreePM	MLFM/MLFV	Data based	Public	119
HACC	TreePM/P ³ M	CRK-SPH	Data based	Private	418
PKDGRAV3	Tree/FM	–	Data based	Public	419
Gasoline2	Tree	SPH	Task based	Public	420
SWIFT	TreePM/FM	SPH	Task based	Public	421

AMR, adaptive mesh refinement; CRK-SPH, conservative reproducing kernel smoothed particle hydrodynamics; FM, fast multipole; MG, multigrid; ML, multilevel; MLFM/MLFV, mesh-free finite mass/finite volume; MMFV, moving-mesh finite volume; P³M, particle-particle particle-mesh; PM, particle-mesh; SPH, smoothed particle hydrodynamics; TreePM, tree + PM. Data-based, data parallelism focuses on distributing data across different nodes, which operate on the data in parallel; task-based, task parallelism focuses on distributing tasks concurrently performed; private, private code; public, publicly available code (in some cases with limited functionality). ^aGravity solver is based on PKDGRAV3. ^bBased on the GADGET-3 code.

on the details of the particle distribution, and no explicit force softening is necessary for this scheme since the force is automatically softened on the grid scale. Combining the particle-mesh method with a set of nested grids of increasing resolution enables an efficient force solver for inhomogeneous systems resulting in adaptive-mesh-refinement schemes. Multigrid or multilevel methods, which solve the discretized form of Poisson's equation using relaxation methods, such as Gauss–Seidel iterations, are also commonly used²⁴. The advantage of this technique over the fast Fourier transform approach is that the grid does not need to be equidistant, but can be locally adapted according to the particle density. The structure of such an adaptively refined mesh is identical to that of a shallow octree.

- *Hybrid schemes.* A variety of schemes combine direct summation-based techniques, for short-range forces, with Fourier transform-based methods, for long-range forces. The most basic example of this is the particle-particle plus particle-mesh method²⁵. A common hybrid scheme is the tree particle-mesh method²⁶ where the direct summation for short-range interactions is approximated by a tree-like method. Combinations of the multigrid method with the fast Fourier transform are also used, where the Fourier transform is used as a force solver on the coarsest grid²⁷. Most modern simulations implement these hybrid solvers to achieve high efficiency.

Beyond the N-body method. Conceptually different methods to solve the collisionless Boltzmann equation have also been developed. However, none of these alternatives have so far been widely used for general structure formation simulations. These different methods are motivated, among other factors, by the desire to resolve the fine-grained structure of the phase-space density and to avoid numerical inaccuracies of the N-body approach

such as the artificial clumping of simulation particles for dark matter models with a cut-off in the initial power spectrum²⁸. Among the methodological alternatives to the N-body method are, for example, a reformulation of the Boltzmann–Poisson system as a Schrödinger equation^{29–31}, the waterbag method^{32,33}, geodesic deviation equation-based methods^{34,35}, Lagrangian tessellation techniques³⁶ and direct integration schemes using finite volume approaches based on positive flux conservation methods of plasma physics³⁷.

Key results of N-body simulations

The earliest dark matter simulations studied halo population models³⁸, the assembly of massive clusters³⁹ and the growth of large-scale structure^{40,41}. Since then, the resolution of these simulations has grown exponentially starting from a few thousand to multitrillion particle simulations⁴². Some selected structure and galaxy formation simulations are listed in TABLE 2. The findings of these simulations can roughly be divided in two categories: the large-scale distribution of dark matter and the structure of dark matter halos. The interaction between baryons and dark matter does affect the structure of dark matter on smaller scales, which is especially important for the internal structure of dark matter halos^{43–49}. Studying these phenomena requires, however, simulations that model both dark matter and baryons.

Large-scale distribution of dark matter. CDM simulations predict that the large-scale distribution of dark matter is not completely homogeneous, but instead exhibits a web-like structure consisting of voids, walls, filaments and halos quantified through, among others, the halo mass and matter correlation functions.

- *Halo mass function.* The halo mass function quantifies the comoving number density of dark matter halos as a function of their virial mass, M_{vir} , typically defined as the mass, M_{200} , enclosed within a radius r_{200} containing a mean density 200 times the critical

Octree

A tree data structure in which each internal node has exactly eight children. Octrees are often used to partition a 3D space by recursively subdividing it into eight octants.

Virial mass

The virial mass is the mass of a gravitationally bound astrophysical system within a spherical region, bounded by the so-called virial radius, where the system obeys the virial theorem.

Table 2 | Recent structure and galaxy formation simulations

Simulation	Volume (Mpc ³)	Method	Mass resolution (M_{\odot})	Spatial resolution (kpc)	Ref.
<i>Dark matter-only</i>					
Millennium	685 ³	TreePM	$1.2 \times 10^9 / -$	6.85/–	422
Millennium-2	137 ³	TreePM	$9.4 \times 10^6 / -$	1.37/–	423
Horizon 4 π	2,740 ³	PM/ML	$7.7 \times 10^9 / -$	10.41/–	424
Bolshoi	357 ³	PM/ML	$1.9 \times 10^8 / -$	1.43/–	425
Full Universe Run	29,167 ³	PM/ML	$1.4 \times 10^{12} / -$	55.6/–	426
Millennium-XXL	4,110 ³	TreePM	$8.5 \times 10^9 / -$	13.7/–	68
MultiDark	1,429 ³	PM/ML	$1.2 \times 10^{10} / -$	10.00/–	427
Dark Sky	11,628 ³	Tree/FM	$5.7 \times 10^{10} / -$	53.49/–	42
v^2 GC	1,647 ³	TreePM	$3.2 \times 10^8 / -$	6.28/–	428
Q Continuum	1,300 ³	TreePM/P ³ M	$1.5 \times 10^8 / -$	2.82/–	70
OuterRim	4,225 ³	TreePM/P ³ M	$2.6 \times 10^9 / -$	6.00/–	418
EuclidFlagship	20,000 ³	Tree/FM	$10^9 / -$	5.00/–	419
Aquarius	Zoom	TreePM	$1.7 \times 10^3 / -$	0.02/–	91
Via Lactea II	Zoom	Tree	$4.1 \times 10^3 / -$	0.04/–	429
GHALO	Zoom	Tree	$1.0 \times 10^3 / -$	0.06/–	408
CLUES	Zoom	TreePM	$3.4 \times 10^5 / -$	0.21/–	430
Phoenix	Zoom	TreePM	$8.7 \times 10^5 / -$	0.21/–	92
ELVIS	Zoom	TreePM	$1.9 \times 10^5 / -$	0.14/–	409
COCO	Zoom	TreePM	$1.6 \times 10^5 / -$	0.33/–	431
<i>Including baryons</i>					
Illustris	107 ³	TreePM+MMFV	$6.7 \times 10^6 / 1.3 \times 10^6$	1.42/0.71	138
Horizon-AGN	142 ³	PM/ML+AMR	$8.0 \times 10^7 / 1.0 \times 10^7$	1.0/1.0	432
EAGLE	100 ³	TreePM+SPH	$9.7 \times 10^6 / 1.8 \times 10^6$	0.7/0.7	111
MassiveBlack-II	143 ³	TreePM+SPH	$1.6 \times 10^7 / 3.2 \times 10^6$	2.64/2.64	411
Bluetides ^a	574 ³	TreePM+SPH	$1.7 \times 10^7 / 3.4 \times 10^6$	0.24/0.24	433
Magneticum	68 ³	TreePM+SPH	$5.3 \times 10^7 / 1.1 \times 10^7$	1.4/0.7–1.4	71
MUFASA	74 ³	TreePM+MLFM	$9.6 \times 10^7 / 1.8 \times 10^7$	0.74/0.74	434
BAHAMAS	571 ³	TreePM+SPH	$5.5 \times 10^9 / 1.1 \times 10^9$	0.25/0.25	435
Romulus25	25 ³	Tree/FM+SPH	$3.4 \times 10^5 / 2.1 \times 10^5$	0.25/0.25	436
IllustrisTNG ^b	111 ³	TreePM+MMFV	$7.5 \times 10^6 / 1.4 \times 10^6$	0.74/0.19	73
Simba ^c	147 ³	TreePM+MLFM	$1.4 \times 10^8 / 2.7 \times 10^7$	0.74/0.74	171
Eris	Zoom	Tree+SPH	$9.8 \times 10^4 / 2 \times 10^4$	0.12/0.12	332
NIHAO	Zoom	Tree+SPH	$3.4 \times 10^3 / 6.2 \times 10^2$	0.12/0.05	112
APOSTLE	Zoom	TreePM+SPH	$5.0 \times 10^4 / 1.0 \times 10^4$	0.13/0.13	437
Latte/FIRE	Zoom	TreePM+MLFM	$3.5 \times 10^4 / 7.1 \times 10^3$	0.02/0.001	335
Auriga	Zoom	TreePM+MMFV	$4.0 \times 10^4 / 6.0 \times 10^3$	0.18/0.18 ^d	286
MACSIS	Zoom	TreePM+SPH	$6.4 \times 10^9 / 1.2 \times 10^9$	5.77/5.77	438
Cluster-EAGLE	Zoom	TreePM+SPH	$9.7 \times 10^6 / 1.8 \times 10^6$	0.7/0.7	113
Three Hundred	Zoom	TreePM+SPH	$1.9 \times 10^9 / 3.5 \times 10^8$	9.59/9.59	439
FABLE	Zoom	TreePM+MMFV	$8.1 \times 10^7 / 1.5 \times 10^7$	4.15/4.15	440
RomulusC	Zoom	Tree/FM+SPH	$3.4 \times 10^5 / 2.1 \times 10^5$	0.25/0.25	441

AMR, adaptive mesh refinement; FM, fast multipole; ML, multilevel; MLFM, mesh-free finite mass; MMFV, moving-mesh finite volume; P³M, particle-particle particle-mesh; PM, particle-mesh; SPH, smoothed particle hydrodynamics; TreePM, tree + PM. In the mass resolution column, the highest resolution is quoted (dark matter/gas). In the spatial resolution column for particle-based codes, the minimum softening length is reported; for mesh codes, the minimum cell size is quoted (dark matter/gas). ^aFinal redshift $z = 8$; spatial resolution is in physical units at that redshift. ^bIllustrisTNG consists of three main simulations: TNG50, TNG100, TNG300; numbers are quoted for TNG100. ^cNumbers for largest volume simulation quoted. ^dFor baryons, the minimum physical softening is reported.

density of the Universe. Other halo boundary definitions such as the splashback radius^{50,51} have been proposed to avoid, for example, the pseudo-evolution of the halo mass and radius⁵². In simulations, dark matter halos are identified through cluster-finding methods such as the friend-of-friends algorithm⁵³ and its extensions based on gravitational unbinding⁵⁴ or phase-space structure finding also taking into account velocity space information⁵⁵. In the CDM cosmogony, structure forms through the hierarchical merging of dark matter halos⁵³, and the corresponding evolution of the halo mass function has been studied extensively^{38,56–63}. Most importantly, these studies revealed that the low-mass end of the halo mass function has a power-law slope close to -2 . Furthermore, the high-mass end of the halo mass function is exponentially suppressed. The halo mass function is also an important probe of the nature of dark matter since many particle candidates predict strong, scale-dependent deviations from the expectations of the CDM model^{64,65}. The high-mass shape and evolution of the halo mass functions also constrains cosmological parameters⁶⁶. Simulation-based empirical halo mass functions are often expressed as $Mdn/dM = \rho_0 d\ln\sigma^{-1}/dMg(\sigma(M))$, where n is the number density, ρ_0 is the mean mass density of the Universe, $\sigma(M)$ is the variance of the linear density field within a top-hat filter containing mass M and $g(\sigma)$ is a function that is determined empirically by fitting the simulation results. This functional form of the halo mass function is motivated and also predicted by the analytic Press–Schechter model³⁸. However, the shape of $f(\sigma)$ found in simulations differs significantly from the analytic model originally proposed in REF.³⁸, agreeing much better with a version motivated by ellipsoidal rather than spherical collapse⁶⁷. The detailed form of $f(\sigma)$ depends, among others, on the simulation details and the halo mass definitions, and a variety of empirical fitting functions have been published^{63,68–71}.

- **Dark matter distribution.** A major success of CDM simulations is their ability to predict the matter distribution on large scales⁷², which is described through the two-point correlation function $\xi(r)$. For a set of points, this function is defined as $\xi(r) = \langle N_p \rangle / N_m - 1$, where $\langle N_p \rangle$ indicates the average number of pairs in a thin shell of radius r centred on one point of the set and N_m indicates the expected number of pairs in the same shell given a uniform distribution of points. Although this function can be estimated analytically in the linear regime, dark matter simulations are needed to probe its evolution in the nonlinear regime. The dark matter correlation function signal grows with time and develops a characteristic shoulder at small scales⁷³. This effect can be explained by the relative contribution of the one-halo term (pairs composed of particles within the same halo) and the two-halo term (pairs formed by particles in different halos) to the clustering signal⁷⁴. Finally, the dark matter correlation function has a markedly different shape than the galaxy correlation function. The latter has a power-law-like shape over a significant

range of scales and a nearly constant amplitude at all redshifts⁷². Indeed, galaxies trace the highest peaks of the dark matter distribution, and their clustering does not change significantly with time, as more and more dark matter structures grow. This bias needs to be taken properly into account when estimating the large-scale total matter distribution using galaxy tracers⁷⁵.

Structure of dark matter halos. CDM simulations have also established multiple characteristics of the dark matter distribution within collapsed and virialized dark matter halos. This has most importantly led to the discovery of a nearly universal radial density profile of dark matter halos.

- **Internal halo structure.** The dark matter mass distribution within halos is well described by a near-universal spherically averaged density profile, the so-called Navarro–Frenk–White profile^{76,77}: $\rho(r) = \rho_s / [(r/r_s)(1 + (r/r_s))^2]$ with a characteristic density ρ_s and a transition radius r_s . This form of density profiles has been shown to arise also in the absence of hierarchical growth such as, for example, in hot dark matter models²⁸ or models with truncated initial power spectra⁷⁸. The central slope of dark matter halos has been debated for a long time and is also affected by baryonic physics effects that require hydrodynamical simulations. More recent higher-resolution simulations found a central slope shallower than -1 , indicating that the density profile is better described by a functional form with a gradually changing slope profile⁷⁹: $\ln(\rho(r)/\rho_{-2}) = (-2/\alpha)[(r/r_{-2})^\alpha - 1]$ with slope α and transition radius r_{-2} . This profile had previously been used to fit star counts in the Milky Way⁸⁰, and is known as the Einasto profile. The adjustable shape parameter, α , shows considerable scatter, but increases systematically with halo mass at $z=0$. The ratio of the virial radius, r_{vir} , and the transition radius, r_s , is called the concentration parameter, c , which correlates with the mass of the halo leading to the mass–concentration relation^{81–83} ($c \propto M^{-\delta}$, $\delta \approx 0.1$). Simulations demonstrated that the dependence of halo concentration on mass, initial fluctuation spectrum and cosmological parameters all reflect a dependence of concentration on the actual halo formation time⁷⁷. Specifically, lower-mass halos typically assemble earlier, and thus have higher concentration, due to the higher density of the Universe at the time of their formation. The shapes of the halos have also been studied, and they depart from sphericity, with halos typically being prolate and increasingly so towards their centres. Major-to-minor axis ratios of two or greater are not uncommon, and more massive halos tend to be less spherical than lower-mass halos^{84–86}. The exact shapes of dark matter halos also depend on the dark matter particle physics model. Simulations also provide information on the velocity structure of halos. The averaged velocity anisotropy profile, $\beta(r) = 1 - 0.5\sigma_t^2/\sigma_r^2$, grows from zero, that is, isotropic, to about 0.5, that is, mild radial anisotropy, towards the outer regions^{87,88}. Here, σ_t denotes the

tangential and σ_r the radial velocity dispersion, with the total velocity dispersion being $\sigma^2 = \sigma_t^2 + \sigma_r^2$. A β value of 1 and $\beta \rightarrow -\infty$ correspond to systems where dark matter particles have purely radial and purely circular orbits, respectively. Simulated dark matter halos therefore turn out to be almost isotropic in their inner regions and to be somewhat radially biased at larger radii. Although both $\rho(r)$ and $\sigma(r)$ are not close to a power law, the combination $f(r) = \rho(r)/\sigma^3(r)$, also called pseudo-phase-space density, is remarkably close to a power law, with slope ≈ -1.875 (REF⁸⁸). This power-law index is identical to that of solutions for self-similar infall onto a point mass from an otherwise uniform Einstein–de Sitter universe⁸⁹.

- **Halo substructure.** As the resolution of dark matter simulations increased, halos within halos, so-called subhalos, could be resolved^{78,90}. Subhalos have cuspy, Navarro–Frenk–White-like density profiles, but they tend to be less extended than comparable halos in the field due to tidal stripping^{87,91}. Bound subhalos with $\mu = M_{\text{sub}}/M_{\text{vir}} > 10^{-7}$ contain about 10% of the halo mass within the virial radius⁹¹. μ is the subhalo mass in units of the virial mass, and M_{sub} is the absolute subhalo mass. Lower-mass halos tend to have fewer subhalos and lower subhalo mass fractions at a given μ . This shift is due to the difference in the relative dynamical age of halos; for example, substructure is more effectively destroyed by tides in older, galactic halos compared with more massive galaxy cluster halos. The cumulative subhalo mass function is a power law $N(>\mu) \propto \mu^{-s}$ for $\mu \ll 1$, with parameter s close to the critical value of unity^{91,92}. For $s = 1$, each logarithmic mass bin contributes equally to the total mass in substructure. This is logarithmically divergent as μ approaches zero, and implies that a significant fraction of the mass could, in principle, be locked in halos too small to be resolved by the simulations. This can, for example, have important implications for the prediction of dark matter annihilation signals since these small unresolved halos can boost the overall resolved annihilation emission⁹³. The abundance of subhalos also varies systematically with other properties of the parent halo, like, for example, the concentration leading to a lower amount of substructure with increasing halo concentration⁹⁴. The radial distribution of subhalos varies only little with the mass or concentration of the parent halo. It is much less centrally concentrated than the overall dark matter profile⁹¹.

Simulating baryons

Dark matter and dark energy dominate the energy budget of the Universe, but the visible components of galaxies consist of baryons. Simulating baryons is therefore crucial to make predictions for the visible Universe. Initially, the baryon component is solely composed of gas, mostly hydrogen and helium. Some of this gas eventually turns into stars during structure formation. Astrophysical gases in cosmological simulations are typically described as inviscid ideal gases following the Euler equations, which can be expressed in different forms leading to different numerical discretization

schemes (BOX 1). Including hydrodynamics in cosmological simulations is numerically demanding due to the large dynamic range, highly supersonic flows and large Reynolds numbers.

Numerical techniques

The hydrodynamical equations can be discretized in different ways using methods that roughly fall into three classes: Lagrangian, Eulerian or arbitrary Lagrangian–Eulerian techniques. The Lagrangian specification of the field assumes an observer that follows an individual fluid parcel (with its own properties such as density) as it moves through space and time. In contrast, the Eulerian specification focuses on specific locations in space through which the fluid flows as time passes. In addition, numerical approaches can also be distinguished between mesh-free and mesh-based algorithms. Mesh-free methods do not require connections between nodes, but are rather based on interactions of each node with its neighbours. An overview of some selected simulation codes and their hydrodynamical simulation techniques is shown in TABLE 1.

Eulerian methods. Eulerian methods are the traditional way to solve the system of hyperbolic partial differential equations. The most common approaches include finite volume, finite difference, finite element, spectral or wavelet methods. For example, accurate Godunov finite volume schemes offer high-order spatial accuracy, have negligible post-shock oscillations and low numerical diffusivity. For these methods, a Riemann problem is solved across cell faces, which yields the required fluxes at each cell face to update the conserved quantities. If the cell is assumed to have uniform properties, this is called a first-order Godunov solver. Modern implementations use parabolic interpolation, known as the piecewise parabolic method^{95,96}. The large dynamic range of cosmological simulations requires adaptive meshes, where the mesh size can be reduced based on some refinement criterion. This leads to the class of adaptive-mesh-refinement schemes^{97–100}, which were first developed for solving general problems involving hyperbolic partial differential equations, and then later were also applied to cosmological simulations. Discontinuous Galerkin methods^{101–103} have become more popular in computational astrophysics since they offer a framework for discretizing hyperbolic problems at any order of spatial accuracy, together with attractive data locality by combining features of spectral element and finite volume methods.

Lagrangian methods. Smoothed particle hydrodynamics is a widely used mesh-free Lagrangian technique for approximating the continuum dynamics of fluids through the use of sampling particles, which may also be viewed as interpolation points, following the equations of motion derived from the hydrodynamical equations^{104–107}. Energy, linear momentum, angular momentum, mass and entropy, assuming no artificial viscosity operates, are all simultaneously conserved. The local resolution follows the mass flow, which is convenient to represent large density contrasts. Over recent

Riemann problem

A specific partial differential equation initial value problem composed of a conservation equation together with piecewise constant initial data, which has a single discontinuity in the domain of interest.

years, various improved formulations of the smoothed particle hydrodynamics method have been developed and applied to cosmological simulations^{108–113}. A few cosmological simulations have also used Lagrangian mesh-based hydrodynamics schemes, which are based on grid deformation techniques^{114,115}.

Arbitrary Lagrangian–Eulerian methods. For arbitrary Lagrangian–Eulerian methods, the grid velocity can be chosen freely. For astrophysical applications, such a scheme has recently been realized through a Voronoi tessellation of a set of discrete mesh-generating points, which are allowed to move freely¹¹⁶. A finite volume hydrodynamic scheme with the Voronoi cells as control volumes can then be consistently defined. Most importantly, due to the mathematical properties of the Voronoi tessellation, the mesh continuously deforms and changes its topology as a result of the point motion, without ever leading to problematic mesh-tangling effects. Similar methods have over recent years also been implemented in other simulation codes^{117,118}. New types of arbitrary Lagrangian–Eulerian, mesh-free, finite mass and finite volume methods have been successfully applied to astrophysical and galaxy formation problems¹¹⁹.

Baryonic physics

The hydrodynamical equations have to be complemented by various astrophysical processes that shape the galaxy population. Most of these processes are implemented through effective, so-called subresolution models, which are necessary due to the limited numerical resolution of simulations.

Gas cooling. Gas dissipates its internal energy through cooling processes, such as collisional excitation and ionization, inverse Compton, recombination and free-free emission. Cooling processes are coupled to the energy equation using cooling functions that are either tabulated or extracted from chemical reaction networks. Cosmological simulations often assume that the gas is optically thin and in ionization equilibrium and neglect three-body processes that are typically unimportant. In addition to primordial cooling, cooling due to heavy elements, so-called metals, is also important. Metal line cooling dominates for temperatures, T , in the range $10^5 \lesssim T \lesssim 10^7$ K. Early simulations typically used cooling rates assuming collisional ionization equilibrium¹²⁰, but the majority of later galaxy formation models account for the photoionization of metals by the metagalactic radiation field¹²¹. For most post-reionization simulations, this metagalactic radiation field is assumed to be spatially uniform, but time dependent¹²². Simulations that resolve the cold phase of the interstellar medium also include gas cooling below 10^4 K via fine-structure and molecular cooling. In neutral atomic gas, the efficiency of cooling is sensitive to the residual ionization degree. In molecular gas (number density $n \gtrsim 100$ cm^{−3}, $T \lesssim 50$ K), the CO molecule dominates the cooling at low densities whereas at higher densities C_2 , O_2 and H_2O start to contribute¹²³. Gas cooling is a direct physical process that is not implemented through a subresolution model. However, following all

cooling processes in detail requires sufficient numerical resolution to resolve the different gas phases.

Interstellar medium. Carefully modelling the interstellar medium is important since its properties directly impact star formation. However, simulating the interstellar medium is challenging due to its complex multiphase structure including magnetic fields and relativistic particles. In particular, modelling the cold phase is technically difficult because of the short timescales associated with the dense gas. These timescales require very small time steps to reliably follow the cold gas evolution. Moreover, the implementation of additional physical processes is needed to accurately model such a phase. To circumvent this problem, this dense gas phase is often not directly modelled, but rather described by an effective polytropic equation of state^{124–126}; for example, $T \propto \rho^{\gamma(p)}$ (where γ is the heat capacity ratio), which naturally emerges from an equilibrium two-phase interstellar medium where a hot, supernova-heated and volume-filling phase coexists with a colder phase containing the bulk of the mass¹²⁴. Other modelling efforts started to abandon the effective equation of state approach and instead aimed towards resolving the multiphase structure directly. Such simulations are starting to be able to resolve the Jeans mass of the gas, corresponding to the scale of molecular cloud complexes. Therefore, a more direct modelling of the multiphase interstellar medium is possible¹²⁷. In such simulations, the gas density and temperature distributions follow a multimodal distribution^{127–129}. In general, the cold gas phase dominates (~90%) the gas mass budget, but occupies a very small volume fraction (~1%), which is mostly composed of hotter gas¹³⁰. Simulating the molecular phase of the interstellar medium is challenging because it requires detailed modelling of the interaction between gas, dust and radiation, which tends to destroy molecules unless gas is able to effectively self-shield from ionizing radiation¹³¹. Detailed models of the interstellar medium must also take into account the various feedback sources that ultimately shape the structure of the interstellar medium. Thus, future simulations should consider how the complex interplay of such a wide range of physical processes affects the properties of the interstellar medium.

Star formation. Cold and dense gas eventually forms stars, and simulations therefore transform a portion of this gas into collisionless star particles, representing coeval, single-metallicity stellar populations described by an underlying initial stellar mass function. Observations support a nearly universal star formation efficiency in molecular gas, where about 1% of the gas is converted into stars per free-fall time^{132,133}. Based on a calculated star formation rate, the gas is converted into star particles typically using a probabilistic sampling scheme. The star formation rate is usually computed based on a Kennicutt–Schmidt type relation as $dM_{\star}/dt = \epsilon M_g/t_{\text{ff}}$, where M_g is the gas cell/particle mass, t_{ff} is the gravitational free-fall time and ϵ is a conversion efficiency typically in the range 0.01–1.00 (REFS^{124,134,135}). However, not all the gas elements are eligible for star formation. Commonly adopted criteria are based on: a density threshold^{111,112,124,134–139}, restricting

Voronoi tessellation
A subdivision of space into convex cells.

Jeans mass
Threshold mass above which a self-gravitating system becomes unstable and begins to collapse.

star formation to gravitationally bound regions identified via the virial parameter — which quantifies the degree of pressure support against gravitational collapse^{135,140}, Jeans length-based criteria, that is, gas must be prone to gravitational instability^{135,137,141,142}, restricting star formation to the molecular gas phase^{134,135,143–147}, or converging flows¹³⁶. As an alternative to the probabilistic sampling scheme, and to better model the clustered nature of star formation, a few simulations also consider star clusters as the unit of star formation by allowing the growth of star particles through accretion from the ambient medium¹⁴⁸. Once stellar particles have been formed, modern galaxy formation models also track the stellar evolution and mass return of these stars to the gas component. This leads to an enrichment of the gas with metals. Early models tracked only type II supernova enrichment, but later models also follow asymptotic giant branch stars¹⁴⁹, type Ia supernovae, which are important for iron enrichment¹⁵⁰, and neutron star mergers for r-process element enrichment¹⁵¹. The actual enrichment is based on metal yield models derived from detailed stellar evolution calculations. These yields are, however, still rather uncertain, at least by a factor of two, particularly at low metallicities and for more massive stars. This uncertainty then propagates into predictions for metal abundances in simulations. Future cosmological simulations will still have to implement star formation as subresolution models with individual stars as their building blocks.

Stellar feedback. Stars interact with their surrounding gas through the injection of energy and momentum leading to a feedback loop regulating star formation. To regulate star formation, stellar feedback must be efficient in launching galactic-scale outflows to eject gas from galaxies, and a variety of subresolution schemes exists to achieve an efficient generation of galactic winds. Those differ in the way energy and momentum, most notably in the form of supernova explosions, are coupled to the surrounding gas. Essentially, the energy can be deposited thermally or kinetically. In the first case, excessive radiative gas cooling must be avoided in the simulation. Although cooling in dense and cold gas is physically expected, at the comparatively low resolution of cosmological simulations it cannot be modelled reliably. The result is then an artificial excessive cooling of the gas, which leads to the unphysical loss of the supernova feedback energy via radiation and greatly reduces its effectiveness. Some approaches therefore disable the radiative cooling of the affected gas for a prescribed amount of time ($\sim 10^7$ yr)¹³⁶, or heat the gas probabilistically¹²⁶ to reach high enough temperatures ($T \sim 10^6$ K) for radiative cooling to become ineffective on timescales of $\sim 10^7$ yr. In the second case, kinetic energy cannot be radiated away until it thermalizes. However, the use of hydrodynamically decoupled galactic wind particles, to realize a non-local injection of momentum in the gas surrounding active star-forming regions, can still be necessary to obtain large-scale galactic outflows^{124,139,150,152}. More explicit models for stellar feedback have been developed. In addition to supernova feedback, they also take into account other feedback channels, such as energy and momentum injection by stellar winds and

photoionization and radiation pressure due to radiation emitted by young, massive stars^{128,134,135,153,154}. The combination of these processes then leads to a regulation of star formation to the observed low gas to star conversion efficiency of 1% per free-fall time^{132,133}. Stellar feedback must be efficient in launching galactic-scale outflows to eject gas from galaxies, thereby also explaining the low baryon retention fraction in galaxies^{155,156}. Explicit feedback models can make direct predictions for the outflow rates of these outflows¹⁵⁷, whereas older models typically prescribe the mass loading of these galactic-scale outflows close to the galaxies. Subresolution models of stellar feedback vary widely among different galaxy formation models. More work is required to understand in detail which stellar feedback channels are most important for shaping the different types of galaxies.

Supermassive black holes. Supermassive black holes are observed in massive galaxies^{158,159}, in small, bulge-less disc galaxies^{160,161} and in dwarf galaxies^{162,163}. Simulations therefore include models for supermassive black holes, and numerically seed them typically in dark matter haloes with masses $\gtrsim 10^{10} - 10^{11} M_\odot$, where M_\odot denotes the solar mass, since the true seeds cannot be resolved, and their origin is not yet fully understood. They then accrete mass often based on an Eddington-rate-capped Bondi–Hoyle-like accretion rate: $\dot{M}_{\text{BH}} = (4\pi G^2 M_{\text{BH}}^2 \rho) / (c_s^2 + v_{\text{rel}}^2)^{3/2}$, where M_{BH} is the black hole mass, ρ and c_s are the gas density and gas sound speed, respectively, and v_{rel} denotes the relative velocity between the gas and the black hole. Depending on the numerical resolution, this accretion rate is sometimes artificially increased, possibly in a density-dependent fashion, to compensate for the inability of simulations to resolve the multiphase structure of gas¹⁶⁴. Many simulations also explored variations of the Bondi–Hoyle accretion model to overcome its limitations. The Bondi model, for example, implicitly assumes that the accreting gas has negligible angular momentum, which is most likely unrealistic. Some models therefore assume that black holes might be primarily fed by gas driven to the centres by gravitational torques from non-axisymmetric perturbations¹⁶⁵, which have more recently been explored in simulations^{166–171}. Black holes also grow through mergers, which are modelled in cosmological simulations as well. Due to resolution limitations, general relativistic effects are not taken into account and it is assumed that the black holes of the two galaxies merge instantly once they come close enough, that is, within their numerical accretion radius, which is typically calculated based on a nearest-neighbour search of local gas resolution elements.

Feedback from active galactic nuclei. Active galactic nuclei are related to observational phenomena associated with accreting supermassive black holes including electromagnetic radiation, relativistic jets and less-collimated non-relativistic outflows¹⁷². The resulting energy and momentum coupling with the surrounding gas leads to the regulation of black hole growth and star formation in more massive halos ($M \gtrsim 10^{12} M_\odot$). This feedback is commonly divided in two modes (quasar and

r-process

The abbreviation of ‘rapid neutron-capture nuclear process’, whereby a nucleus rapidly increases its atomic number by repeatedly capturing neutrons.

radio mode) that are implemented differently in simulations. However, some galaxy formation models do not make this distinction, arguing that cosmological simulations lack the resolution to properly distinguish the two feedback modes, and to limit the number of feedback channels to the minimum required to match the observational data¹¹¹. Quasar mode feedback is associated with the radiatively efficient mode of black hole growth and is often implemented through energy or momentum injection assuming that the bolometric luminosity is proportional to the accretion rate, and a fixed fraction of this luminosity is deposited into the neighbouring gas^{173,174}. Momentum-driven winds via radiation pressure on dust have been implemented in REFS^{175–177} and via broad-line-region winds in REF¹⁷⁸. Radio-mode feedback is caused by highly collimated jets of relativistic particles, which are often associated with X-ray bubbles with enough energy to offset cooling losses. Therefore, this feedback mode is assumed to be important for the regulation of star formation in massive galaxies. Radio-mode feedback is often implemented as a second subresolution feedback channel once the accretion rate is below a critical value^{179,180}. Jets themselves cover an enormous dynamic range, being launched at several Schwarzschild radii, and propagating outwards to tens of kiloparsecs. Directly resolving them in detail in cosmological simulations is therefore currently not feasible. The subresolution models for supermassive black holes are therefore still very uncertain since they have to bridge a very large-scale gap between the actual accretion and feedback, and the scales that can be resolved with simulations.

Magnetic fields. Magnetic fields permeate the Universe on all scales and impact the motion of ionized gas. Conversely, gas dynamics affects the topology and strength of the magnetic fields. Cosmological simulations typically use the ideal magnetohydrodynamics approach, which is a good approximation for cosmological magnetic fields (BOX 2). This approach assumes that the plasma is perfectly conducting and that relativistic effects, that is, terms $\propto (v/c)^2$, with v being the velocity, such as the displacement current $c^{-1}\partial\mathbf{E}/\partial t$, with \mathbf{E} being the electric field, are negligible. However, for other situations, the ideal magnetohydrodynamics approximation breaks down and non-ideal terms, such as ohmic resistivity, ambipolar diffusion and the Hall effect, must be taken into account. These effects are important, especially at very small spatial scales, for example, for individual star formation, causing a diffusion of the magnetic field. On large cosmological scales, the impact of magnetic fields on the dynamics of gas is rather limited¹⁸¹. However, magnetic fields are an essential constituent of the interstellar medium, providing both pressure support against gravity¹⁸² and influencing the propagation of cosmic rays¹⁸³. Cosmological simulations including magnetic fields through the ideal magnetohydrodynamics are typically initialized with a certain magnetic seed field, since the approximations and assumptions of ideal magnetohydrodynamics do not permit the self-consistent generation of magnetic fields. Some simulations also consider source terms such as the Biermann battery effect or field injection from

stellar winds as the source for initial magnetic fields¹⁸⁴. However, in most cases, the initial conditions of such cosmological simulations contain a small seed field of the order of roughly 10^{-10} gauss at a redshift of around $z \sim 100$. The simulation results are not sensitive to this seed field as long as its value is not too large, close to violating observational constraints^{181,185}, or vanishingly small. The reason for this insensitivity lies in the strong amplification processes that occur during structure formation. This amplification typically occurs in two phases. At high redshifts, a turbulent dynamo leads to an exponential amplification of the magnetic fields in halos. Once the initial turbulent amplification phase has saturated, a second phase of magnetic field amplification starts, leading to a linear growth caused by a galactic dynamo¹⁸⁶. The numerical discretization of the ideal magnetohydrodynamics equations is challenging because of the solenoidal constraint $\nabla \cdot \mathbf{B} = 0$, where \mathbf{B} is the magnetic field. Two main families of discretization techniques exist: divergence cleaning schemes and constrained transport. For the cleaning approach, source terms are added to the underlying magnetohydrodynamics equations to correct for divergence errors^{187,188}. Constrained transport discretizations¹⁸⁹ guarantee that the divergence is zero by construction. However, a more complex implementation is required in this situation. For instance, vector potentials¹⁹⁰, Euler potentials^{191,192} or staggered discretizations of the magnetic field components^{193–197} must be used.

Cosmic rays. Relativistic nuclei and electrons, known as cosmic rays, are another important component of the galactic ecosystem. They are accelerated through diffusive shock acceleration, mostly in supernova remnants and jets of active galactic nuclei (first-order Fermi acceleration) and turbulence (second-order Fermi acceleration). Cosmic rays contribute to the pressure in the interstellar medium^{198,199}, provide an important heating channel^{200,201} and potentially play a role in driving galactic gas outflows^{202–211} due to their shallow equation of state ($P_{\text{cr}} \propto \rho_{\text{cr}}^{4/3}$), where P_{cr} is the cosmic ray pressure and ρ_{cr} is the cosmic ray density, their long cooling time, and their ability to transfer energy to outflows outside of star-forming discs²¹² (BOX 2). The propagation of cosmic rays is dictated by the strength and topology of the underlying magnetic fields. Reliably modelling the propagation of cosmic rays therefore requires a detailed modelling of magnetic fields. To capture all these effects self-consistently, the injection, acceleration and transport of cosmic rays, through anisotropic diffusion and streaming, must be included in the simulations. This requires, in principle, a detailed knowledge of the cosmic ray energy spectrum to accurately estimate energy losses and heating rates. The discretization of the cosmic ray transport terms is difficult. For example, anisotropic diffusion requires discretization techniques that avoid the violation of the entropy condition by limiting the transverse fluxes^{206,213–215}. Modelling cosmic ray streaming is particularly challenging because of the discontinuous dependence of the streaming velocity on the sign of the scalar product between the magnetic field and the cosmic ray pressure gradient in the one-moment

Biermann battery

A process by which a weak seed magnetic field can be generated from zero initial conditions.

Galactic dynamo

A theory describing how a conducting and rotating fluid can build and sustain a magnetic field over galactic scales.

Box 2 | Modelling

Modelling cosmic magnetic fields

- Ideal magnetohydrodynamics (MHD) equations

$$\frac{\partial \rho}{\partial t} + \nabla \cdot (\rho \mathbf{v}) = 0$$

$$\frac{\partial \rho \mathbf{v}}{\partial t} + \nabla \cdot (\rho \mathbf{v} \otimes \mathbf{v} + P \mathbf{I}) = \frac{\mathbf{J} \times \mathbf{B}}{c}$$

$$\frac{\partial (\rho e + e_B)}{\partial t} + \nabla \cdot \left[(\rho e + P) \mathbf{v} + c \frac{\mathbf{E} \times \mathbf{B}}{4\pi} \right] = 0$$

- MHD Maxwell equations

$$\nabla \times \mathbf{B} = \frac{4\pi}{c} \mathbf{J}$$

$$\frac{1}{c} \frac{\partial \mathbf{B}}{\partial t} + \nabla \times \mathbf{E} = 0$$

$$\nabla \cdot \mathbf{B} = 0$$

$$\mathbf{E} = -\frac{\mathbf{v} \times \mathbf{B}}{c}$$

The evolution of the magnetic field, \mathbf{B} , is given by the induction equation, $\partial \mathbf{B} / \partial t = \nabla \times (\mathbf{v} \times \mathbf{B})$. Magnetic fields act on gas through the Lorentz force, $\mathbf{J} \times \mathbf{B} / c$ with the current density, $\mathbf{J} = c \nabla \times \mathbf{B} / (4\pi)$. The energy equation contains the magnetic energy density, $e_B = ||\mathbf{B}||^2 / 8\pi$, and the Poynting vector, $c(\mathbf{E} \times \mathbf{B} / 4\pi)$, in the flux part.

Modelling cosmic rays

- Ideal magnetohydrodynamics equations with cosmic rays

$$\frac{\partial \rho}{\partial t} + \nabla \cdot (\rho \mathbf{v}) = 0$$

$$\frac{\partial \rho \mathbf{v}}{\partial t} + \nabla \cdot (\rho \mathbf{v} \otimes \mathbf{v} + P \mathbf{I}) = \frac{\mathbf{J} \times \mathbf{B}}{c} - \nabla P_{cr}$$

$$\frac{\partial (\rho e + e_B)}{\partial t} + \nabla \cdot \left[(\rho e + P) \mathbf{v} + c \frac{\mathbf{E} \times \mathbf{B}}{4\pi} \right]$$

$$= -(\mathbf{v} + \mathbf{v}_{st}) \cdot \nabla P_{cr} + \Lambda_{th} + \Gamma_{th}$$

- MHD Maxwell equations

$$\nabla \times \mathbf{B} = \frac{4\pi}{c} \mathbf{J}$$

$$\frac{1}{c} \frac{\partial \mathbf{B}}{\partial t} + \nabla \times \mathbf{E} = 0$$

$$\nabla \cdot \mathbf{B} = 0$$

$$\mathbf{E} = -\frac{\mathbf{v} \times \mathbf{B}}{c}$$

- Cosmic rays energy density evolution

$$\frac{\partial \varepsilon_{cr}}{\partial t} + \nabla \cdot \left[\varepsilon_{cr} (\mathbf{v} + \mathbf{v}_{st}) - \kappa_e \mathbf{b} (\mathbf{b} \cdot \nabla \varepsilon_{cr}) \right]$$

$$= -P_{cr} \nabla \cdot (\mathbf{v} + \mathbf{v}_{st}) + \Lambda_{cr} + \Gamma_{cr}$$

Cosmic rays exhibit a force on the gas through ∇P_{cr} . Their energy density is influenced by streaming with velocity \mathbf{v}_{st} ($\varepsilon_{cr} (\mathbf{v} + \mathbf{v}_{st})$), anisotropic diffusion with coefficient $\kappa_e (\mathbf{b} \cdot \nabla \varepsilon_{cr})$, and adiabatic processes due to the compression of the Alfvén frame ($P_{cr} \nabla \cdot (\mathbf{v} + \mathbf{v}_{st})$). cr stands for cosmic ray and th for thermal. Source terms are identified with Γ and the sink terms with Λ .

Modelling cosmic radiation fields

- Radiation hydrodynamics equations

$$\frac{\partial \rho}{\partial t} + \nabla \cdot (\rho \mathbf{v}) = 0$$

$$\frac{\partial (\rho \mathbf{v})}{\partial t} + \nabla \cdot (\rho \mathbf{v} \otimes \mathbf{v} + P \mathbf{I}) = \Gamma_p$$

$$\frac{\partial (\rho e)}{\partial t} + \nabla \cdot (\rho e \mathbf{v}) = -\Lambda + \Gamma_E$$

- Radiative transfer equation

$$\frac{1}{c} \frac{\partial I_\nu}{\partial t} + \mathbf{n} \cdot \frac{\partial I_\nu}{\partial \mathbf{r}} = -\kappa_\nu I_\nu + j_\nu$$

The radiative transfer equation relates the specific radiation intensity, I_ν , with the absorption coefficient, κ_ν , and the specific emissivity, j_ν . The radiation direction of propagation is represented by the unit vector \mathbf{n} . Λ is the cooling function, and Γ_p and Γ_E are source terms that describe the transfer of momentum and energy from the radiation to the gas. ρ is the density, c is the speed of light, ν is the frequency, ε_{er} is the cosmic ray energy density, \mathbf{v} is the velocity, P is the pressure, $\mathbf{b} = \mathbf{B} / ||\mathbf{B}||$ is the B field direction and e is the specific (per unit mass) gas total energy.

formulation of cosmic ray hydrodynamics. This leads to unphysical oscillations of the solution and small time steps, especially near cosmic ray pressure maxima, if not addressed in form of regularization techniques — such as replacing the sign function with the hyperbolic tangent function that ensures a smooth dependence of the streaming velocity on cosmic rays and gas properties^{208,215,216}, albeit at the expense of a dependence of the solution on a numerical parameter. An elegant solution of this problem is to replace the equation for the cosmic ray energy by two equations for cosmic ray energy and flux that are coupled to the magnetohydrodynamics system of equations^{217,218}. This two-moment formulation can be derived from quasi-linear theory of cosmic ray transport and describes cosmic ray streaming and diffusion self-consistently with a hyperbolic set of equations, which also contains the evolution equations for Alfvén waves that are self-generated by the streaming cosmic rays²¹⁸.

Radiation hydrodynamics. Radiation alters the thermal, kinetic and chemical state of the gas. Radiation hydrodynamics simulations are required to capture this self-consistently. In the context of cosmological simulations, radiation hydrodynamics simulations have so far primarily been used to study the epoch of reionization^{142,219,220}. These simulations are aimed at exploring the high-redshift Universe and are typically not evolved towards the low-redshift regime. Consequently, the galaxy formation models used in these simulations cannot be tested against low-redshift predictions. Only a limited number of simulations have studied the impact of radiation in the context of galaxy formation simulations^{129,221}. The main reason for this lack of detailed radiation hydrodynamics studies is that numerical radiative transfer is challenging because of the high dimensionality caused by the frequency and directional dependencies of photon propagation (BOX 2). Even more challenging is the fact that, in general, the speed of light poses

severe constraints on the duration of the time steps of these simulations, which can however be circumvented to some degree through the application of a reduced speed of light approximation^{222–225}. The most common numerical methods for radiation hydrodynamics are ray-tracing, Monte Carlo and moment-based methods. The ray-tracing method discretizes the radiative transfer equation along individual directions from each source. Long characteristic ray-tracing schemes^{226–228} cast rays from the source through the whole simulation domain, and the transport, absorption and emission of radiation is computed along each ray. Long characteristic schemes are accurate, but computationally expensive, since they scale as $\mathcal{O}(N_s \times N_c^p)$, where N_s is the number of sources, N_c is the number of underlying discretization resolution elements, for example, cells, and p is a method- and geometry-dependent exponent^{229,230}. Short characteristic methods^{231–234} solve the radiative transport only along rays that connect nearby cells, allowing an efficient parallelization and merging procedures to break the $\mathcal{O}(N_s \times N_c^p)$ scaling. Monte Carlo methods^{235–240}, often only applied in post-processing, emit photon packets and propagate them, probing the gas opacity, interaction lengths and scattering angles from underlying probability density functions, thus stochastically solving the radiative transfer equation. One drawback of Monte Carlo schemes is that the signal-to-noise ratio improves only as the square root of the number of photon packets due to Poisson noise. Still, Monte Carlo is highly accurate and photon-weighting, path-based estimators and discrete diffusion schemes help overcome the efficiency barriers that inhibit convergence^{241–244}. Moment-based methods have become popular over recent years due to superior scalability^{129,245–248}. They are based on a fluid-like description of radiation fields by taking zeroth, first and second moments of the radiation specific intensity with respect to the angular variable. This defines a radiation energy density E_ν , flux \mathbf{F}_ν , pressure tensor \mathbb{P}_ν and hyperbolic conservation laws for the energy density and the radiation flux (ν is the frequency). Similar to the hydrodynamical case, where an equation of state is required to relate gas pressure and density, a non-unique closure relation is required to relate \mathbb{P}_ν to E_ν and \mathbf{F}_ν . A widely used approach is to define $\mathbb{P}_\nu \equiv E_\nu \mathbb{D}$, where \mathbb{D} is the Eddington tensor that can be estimated with different methods, for example, through flux-limited diffusion^{104,249}, the optically thin variable Eddington tensor approach^{222,250,251} or the M1 closure^{129,245,248,252,253}. For the former methods, \mathbb{D} is estimated assuming that the gas between sources of radiation is always optically thick or thin. The M1 method, instead, computes the Eddington tensor by using local radiation quantities.

Other physics. Additional physical processes considered in some cosmological simulations of galaxy formation are, for example, dust physics^{254–262}, thermal conduction^{177,214,263–267} and viscosity^{268–271}. Dust has typically been neglected in galaxy formation simulations since it contributes only about 1% to the mass budget of the interstellar medium. However, dust plays an important role in the evolution of the interstellar medium, affecting the thermochemistry and radiation processing.

Therefore, galaxy formation simulations began to incorporate simple dust models to follow its production, growth and destruction in the interstellar medium. Most of these implementations treat dust as a passive scalar and model the processes affecting the dust population through effective rate equations. Thermal conduction is another physical effect that is often neglected in cosmological simulations of galaxy formation. However, in hot plasmas of galaxy clusters, conduction can affect the thermodynamic properties of galaxy clusters, as has recently been demonstrated^{267,272–274}. Simulating thermal conduction requires a precise numerical magnetohydrodynamics implementation to resolve the strength and topology of the magnetic field, and an efficient anisotropic diffusion solver to model the conduction²¹⁴.

Caveats and limitations. Simulations of the dark matter component typically boil down to implementing efficient N -body methods and parallelization schemes. Simulations of the baryonic matter component are, however, more challenging, since they require reliable hydrodynamics numerical schemes and well-posed sub-resolution models. These additional complications lead to some caveats and limitations of such simulations.

- **Calibration.** The numerical implementation of baryonic physics is based on subresolution models due to the intrinsic resolution limitations of any simulation. These effective models depend on a certain number of adjustable parameters. Depending on the exact galaxy formation model implementation, these parameters can either be chosen based on physical arguments or they require a certain calibration procedure. The latter approach is often used in large-volume simulations, where the subresolution models are less detailed compared with those of zoom simulations. The calibration process consists of a parameter exploration for the effective models through a large number of simulations. These simulations typically cover a smaller volume compared with production simulations. The calibration is then based on a comparison to some key observables of the galaxy population, such as the star formation rate density as a function of cosmic time, the galaxy stellar mass function at $z=0$ and the present-day stellar-to-halo mass relation.
- **Numerical convergence.** Cosmological simulations have to cover a wide range of spatial and timescales. This implies that simulations have to aim for the highest possible number of resolution elements. However, even state-of-the-art simulations cannot capture all relevant scales. Simulations are therefore often performed at different resolution levels to understand the exact dependence of the results on the number of resolution elements. A simulation prediction is then said to be converged once this prediction does not significantly change anymore if the numerical resolution is further increased.
- **Diverging results.** Various simulations now agree on a wide range of predictions. This is especially the case for predictions of the stellar content of galaxies and related observables. However, there is also a wide range of predictions that diverge among different simulations. For example, the characteristics

Eddington tensor

A tensor relating the radiation pressure to radiative energy for radiative transfer calculations.

of gas around galaxies are very sensitive to the feedback implementations used in the different galaxy formation models. This can lead to rather different outcomes for the thermodynamic structure of gas around galaxies. Such difference can then be used to differentiate and test galaxy formation models.

Key hydrodynamical simulation results

The results of hydrodynamical simulations can directly be confronted with observational data, providing important tests for galaxy formation models. This often involves the construction of detailed mock observations based on the simulated data^{275,276}. Early simulations successfully reproduced properties of the intergalactic medium, such as the column density distribution of the Lyman- α forest²⁷⁷. Many simulations also focused on the formation of individual galaxies^{278–282}. However, such simulations suffered for a long time from, for example, inconsistent stellar masses, galaxy sizes, star formation histories and galaxy morphologies^{152,283–285}. Only over the past decade, simulations have begun to produce realistic galaxies^{73,111,112,135,138,286,287}. However, different subresolution implementations of astrophysical processes remain a major source of uncertainties. Results of hydrodynamical simulations can be grouped into those for global properties for the entire galaxy population and those for the properties of individual galaxies.

Global properties. Large-volume simulations are ideally suited to explore global properties of the galaxy population due to their large statistical sample size. This enables direct comparisons to astronomical galaxy surveys. TABLE 2 lists some selected recent structure and galaxy formation simulations.

- *Stellar content of galaxies.* One of the most fundamental properties of the galaxy population is the galaxy stellar mass function, which quantifies the comoving number density of galaxies as a function of galaxy stellar mass. Stellar mass functions are frequently described by a Schechter function²⁸⁸ with parameter M^* , a characteristic mass scale above which the distribution is exponentially suppressed, a normalization ϕ^* and α^* setting the low-mass slope. Observed low-redshift parameters are roughly given by $\log(M_*/M_\odot) \approx 11$, $\log(\Phi^*/\text{Mpc}^{-3}) \approx -2.7$, $\alpha^* \approx -1.2$ (REF²⁸⁹). However, double Schechter functions provide an even better description of low-redshift galaxy stellar mass functions^{290–294}. The halo mass function exhibits a steeper low-mass slope, ≈ -2 , than the galaxy stellar mass function and the exponential suppression occurs at a lower volume density. Reproducing the observed stellar mass function therefore requires a strong suppression of star formation at both the low- and high-mass ends. Galaxy formation models assume that supernova feedback flattens out the low-mass ($M \lesssim 10^{12} M_\odot$) slope by suppressing star formation^{295–297} whereas the suppression of bright and high-mass ($M \gtrsim 10^{12} M_\odot$) galaxies is regulated by feedback from active galactic nuclei. Energetically plausible forms of supernova and active galactic nuclei feedback in simulations resulted in galaxy stellar mass

functions that are consistent with observational data. Simulation predictions are also often confronted with empirical constraints on the relationship between stellar mass and halo mass, which are derived based on various galaxy-halo mapping techniques^{155,156}. This ratio of stellar mass to halo mass peaks around halo masses of roughly $\sim 10^{12} M_\odot$, where star formation is most efficient. For higher and lower halo masses, the star formation rates are reduced due to feedback processes. Modern large-volume simulations reproduce the stellar-to-halo mass relationship at low and high redshifts reasonably well^{111,298}.

- *Gas around galaxies.* One of the key advantages of hydrodynamical simulations compared with semi-analytic models (BOX 3) is their ability to make detailed predictions for the distribution and properties of gas around galaxies including the circumgalactic medium, the intracluster medium and the intergalactic medium. The circumgalactic and intergalactic media are quite diffuse (density $n \sim 10^{-3} - 10^{-7} \text{ cm}^{-3}$) and cool ($T \sim 10^{4-6} \text{ K}$) and observations in emission, like Lyman- α and metal lines, are therefore rather challenging. However, absorption line observations from background quasars can probe the distribution, enrichment and ionization state of this gas. One of the first successes of hydrodynamical simulations has been the reproduction of the declining trend of the number of absorbing clouds per unit redshift and linear interval of H I column density with column density in the Lyman- α forest²⁷⁷. Reproducing properties of the circumgalactic medium, however, is significantly more challenging. Observations of this gas indicate that it features a rich multiphase structure where individual lines of sight simultaneously contain highly ionized, warm and cool atomic

Box 3 | Semi-analytic modelling of galaxy formation

Studying baryonic physics through hydrodynamical simulations is computationally expensive compared with dark matter-only N -body simulations. An alternative approach is to model baryonic physics on top of N -body dark matter simulations through analytic models. This combination of numerical dark matter-only simulations and analytic models for the prescription of baryonic physics is known as semi-analytic modelling^{442–446}. These semi-analytic models track, for example, how much gas accretes onto halos, how much hot gas cools and turns into stars, or how feedback processes remove cold gas from the galaxy or heat the halo gas. The models are based on the merger history of dark matter halos extracted from N -body simulations. The result of such a calculation is a predicted galaxy population that can be compared to observational data in a similar way to the output of full hydrodynamical simulations. The key advantage of semi-analytical models is their efficiency. It is therefore possible to perform a wide range of calculations, using different model variations. However, a disadvantage of semi-analytic models is that they are less self-consistent compared with hydrodynamical simulations. Furthermore, studying detailed gas properties, for example, the circumgalactic gas, with these models is not directly possible since the gas component is not resolved.

species^{299,300}. The coolest and densest parts of this gas have spatial scales of 10–100 pc (REF.³⁰¹), although the coherence scale can reach up to ~ 1 kpc (REF.³⁰²). These spatial scales are below the typical circumgalactic gas resolution limits of galaxy formation simulations. More recently, cosmological simulations with special circumgalactic gas refinement schemes have been used to overcome some of the resolution limitations. Such simulations increase the numerical resolution in the circumgalactic gas reaching smaller spatial scales^{303–305}. At $z=2$, such simulations can reach a spatial resolution below ~ 100 pc (REF.³⁰⁴), and at $z=0$ below ~ 1 kpc within the circumgalactic medium³⁰³. In addition to resolution concerns, the circumgalactic medium is influenced by feedback-driven outflows from galaxies, whose characteristics are not yet properly understood and modelled. The circumgalactic medium can therefore also be used to constrain feedback mechanisms. The intracluster medium can directly be observed via X-ray observations due to the much higher gas temperatures ($T \sim 10^{7–8}$ K). Many properties of the intracluster medium, such as X-ray and Sunyaev–Zeldovich scaling relations or the iron distribution, can be accurately modelled in simulations^{306–309}. However, significant challenges remain for galaxy formation models to reproduce cluster entropy profiles and, in particular, distinct cool-core and non-cool-core clusters^{113,310}.

- **Galaxy clustering.** Galaxy clustering varies as a function of galaxy mass and galaxy properties, such as formation time, star formation rate and colour. Simulations now reproduce a number of features in the galaxy clustering signal, including the mass-dependent two-point correlation length⁷³, which increases with increasing masses^{311–313}, the clustering signal for non- and star-forming galaxies^{73,314}, and the steepening of the power-law slope γ of the galaxy correlation function with declining redshift ($\gamma \sim 1.8$ at $z \simeq 0$ and $\gamma \sim 1.6$ at $z \simeq 1$ (REFS^{73,315})).
- **Scaling relations.** Galaxies exhibit a wide range of scaling relations linking various observables constituting another important test for galaxy formation models. Modern large-volume hydrodynamical simulations broadly reproduce many galaxy scaling relations including the mass–size³¹⁶, the supermassive black hole mass–stellar velocity dispersion relation³¹⁷ and the mass–metallicity³¹⁸ relation^{319–322}. Also, other galaxy characteristics, such as the colour of galaxies as a function of galaxy stellar mass, can now be reasonably well reproduced by cosmological simulations^{287,323,324}. However, there are still points of tension including, for example, the magnitude of the scatter, the detailed shape of the relation or the dependence on additional galaxy properties.

Sunyaev–Zeldovich scaling relations

Scaling relations connecting galaxy cluster properties, such as mass and luminosity, to the Sunyaev–Zeldovich Compton parameter.

Galaxy properties. The detailed properties of late-type disc-like and early-type spheroid-dominated galaxies have been studied extensively using simulations.

- **Properties of late-type galaxies.** Simulating the formation of star-forming, late-type spiral galaxies has been one of the most pressing challenges of

computational galaxy formation. For a long time, simulations struggled to form galaxies with extended and rotationally supported stellar and gaseous discs as observed in the Universe. These discs are expected to form through angular momentum conservation of the cooling gas in dark matter halos^{325,326}. However, realizing this mechanism in cosmological simulations turned out to be difficult, and early works produced galaxies dominated by a stellar spheroidal component, with a subdominant disc only^{283,327}. More efficient stellar feedback schemes were required to offset runaway radiative losses of the star-forming gas, the so-called overcooling catastrophe³²⁸, and to eject the low-angular momentum material responsible for the creation of the dominant stellar bulge, the so-called angular momentum catastrophe³²⁹. The success of modern simulations in producing late-type disc galaxies is largely due to the ability of stellar feedback to regulate star formation efficiently^{112,134,135,153,286,330–335}. In the past five years, magnetic fields in late-type galaxies have also been studied to understand their topology and field strengths^{186,336–340}. Furthermore, the impact of cosmic rays in galaxies has been studied in more detail over the past decade^{206,208}. These results indicate that cosmic rays are potentially important for driving galactic outflows.

- **Properties of early-type galaxies.** Simulations can also reproduce spheroid-dominated elliptical early-type systems, which broadly match the early formation history³⁴¹, scaling relations (such as the mass and size or velocity dispersion)^{342,343} and the metallicity distribution³⁴⁴ of observed early-type galaxies. The assembly of such large objects proceeds in two phases^{345–348}. At high redshift ($z \gtrsim 1.5$), galaxies grow predominantly *in situ* by efficiently converting gas into stars. At later times, mass is predominantly gained through accretion of smaller substructures (for example, mergers), which also considerably increases galaxy sizes. Spatially resolved spectral observations have shown that spheroid-dominated galaxies have diverse kinematics and shapes. The kinematics is usually described through the so-called spin parameter λ_R . This quantity is used to split galaxies into fast ($\lambda_R > 0.1$) and slow ($\lambda_R < 0.1$) rotator classes. The ellipticity ϵ , instead, is used to define the spheroid's shape. Simulations have played a major role in building a physical picture to explain the diversity in kinematics and shapes of spheroid-dominating galaxies that are produced based on their formation histories^{341,349,350}, in particular, through gas dissipation, which builds rotationally supported structures, and mergers, which set the late-time spin parameter.

Alternative cosmological models

Cosmological simulations of galaxy formation have also been used to explore alternative cosmological models. At the most basic level, the cosmological model can be altered in three different ways: alternative forms of dark matter, alternative forms of dark energy or alternative forms of gravity. We note that many simulations of

alternative cosmological models typically only consider the dark matter component and do not model baryons. However, these simulations then neglect the important backreaction between baryons and dark matter. Similarly, simulations including baryons are also now important to infer cosmological parameters. For example, the Dark Energy Spectroscopic Instrument (DESI), Large Synoptic Survey Telescope (LSST) and Euclid mission will rely on models based on galaxy formation simulations to achieve their forecasted precision. Future explorations of alternative cosmologies have to consider and include these effects by also modelling the baryon component.

Alternative forms of dark matter

A wide range of alternative dark matter models have been proposed over recent decades. However, not all of these models have been studied in detail through simulations. Mostly, three main classes of alternative dark matter models have been simulated: warm dark matter, self-interacting dark matter and fuzzy dark matter. Many of these models have been invoked to address small-scale problems of the CDM paradigm (BOX 4).

Warm dark matter. CDM models exhibit a high- k cut-off in the initial power spectrum due to free-streaming or collisional damping. For a canonical weakly interactive massive particle, this cut-off is of the order of 1 comoving parsec corresponding to a mass scale of $10^{-6} M_\odot$ (REF. ³⁵¹). Warm dark matter (WDM) models have an effective free-streaming length λ_{fs} that scales inversely with particle mass³⁵². For recent cosmologies³, this relation is approximately $\lambda_{\text{fs}} = 33(m_{\text{WDM}}/1\text{ keV})^{-1.11}$ kpc and the corresponding free-streaming mass is $M_{\text{fs}} = 2 \times 10^7 (m_{\text{WDM}}/1\text{ keV})^{-3.33} M_\odot$. The reduction of small-scale power within WDM models has two consequences: first, a reduction of low-mass halos, and second, a reduction of the central density of halos. Simulations of WDM models are typically carried out with the same numerical methods as CDM simulations, but with modified initial conditions. However, the power spectrum cut-off leads to artificial and numerical discreteness effects in N -body simulations²⁸. Special care is then required to avoid a contamination of results in that case. Alternative methods based on phase-space tessellation techniques have been used to study WDM models avoiding these numerical artefacts⁶⁴.

Self-interacting dark matter. Dark matter models that involve dark matter self-interactions^{353,354} have also been explored extensively. Self-interactions are commonly quantified in terms of the cross-section per unit particle mass, σ/m . Models with constant and velocity-dependent cross-sections have both been studied with simulations³⁵⁵. The high central dark matter densities observed in clusters exclude self-interacting dark matter models with $\sigma/m \gtrsim 0.5 \text{ cm}^2 \text{ g}^{-1}$ for these cluster mass scales. More general self-interacting dark matter models have also been suggested. These have both truncated power spectra and self-interactions^{356,357}. Such models affect the internal structure of dark matter halos through the scattering of particles that cause

Box 4 | Small-scale problems of cold dark matter

The cold dark matter paradigm correctly describes the large-scale distribution of galaxies. On subgalactic scales however, some problems have been identified over recent decades⁴⁴⁷. Among the most relevant challenges are: the under-abundance of dwarf galaxies in the Milky Way and in the field (the missing satellites problem)^{78,448–451}, the inconsistency of inner dark matter density profiles in low surface brightness and dwarf galaxies (the cusp–core problem)^{452,453}, the deficit of dark matter in the inner regions of massive dwarf galaxies (the too-big-to-fail problem)^{454,455} and the large variety of shapes of dwarf rotation curves (the diversity problem)⁴⁵⁶. Most of these problems have been found by contrasting dark matter-only simulations with observations, which do not take into account the complex baryonic dark matter interactions. It is therefore possible that these challenges can be solved through the proper modelling of baryonic physics. For instance, the existence of dark matter cores can potentially be explained by the gravitational transfer of energy from supernovae into the orbits of dark matter particles^{457–461}. Alternatively, these discrepancies between observations and cold dark matter simulations can also be explored through alternative dark matter models. These small-scale problems have therefore generated significant interest in the exploration of alternative dark matter scenarios.

the formation of density cores. However, the truncated power spectra also lead, similar to WDM models, to a suppression of halo substructure. Various simulations have demonstrated that models with $\sigma/m \approx 0.5 – 10 \text{ cm}^2 \text{ g}^{-1}$ produce dark matter cores in dwarf galaxies with sizes of $\sim 0.3 – 1.5$ kpc and central densities of $2.0 – 0.2 \times 10^8 M_\odot \text{ kpc}^{-3} = 7.40 – 0.74 \text{ GeV cm}^{-3}$ that can alleviate some CDM small-scale problems^{358–361}. Simulations of self-interacting dark matter are based on the N -body approach coupled to a local Monte Carlo-based probabilistic scattering scheme to model particle self-interactions.

Fuzzy dark matter. An ultralight bosonic scalar field is a completely different alternative to the CDM paradigm³⁶², where a bosonic fluid with a particle mass of $m \sim 10^{-22} \text{ eV}$ suppresses small-scale structure owing to macroscopic quantum properties^{363–365} with a typical de Broglie wavelength of $\lambda_{\text{DB}} \sim 1 \text{ kpc}$ (REFS ^{366,367}). The dark matter fluid forms in this case a cosmological Bose–Einstein condensate^{368–370}. Such an ultralight scalar field of spin 0 at zero temperature is described in the non-relativistic limit by the Schrödinger–Poisson equations^{363,364,371,372}: $i\hbar\partial\psi/\partial t = -\hbar^2/2m\nabla^2\psi + mV\psi$ and $\nabla^2V = 4\pi G(\rho - \bar{\rho})$, where $\rho = |\psi|^2$ is the fluid density, ρ is the density, $\bar{\rho}$ is the mean density and V is the potential with G the gravitational constant. One consequence of the macroscopic quantum behaviour of the fluid is that the fluid admits stable, minimum-energy soliton configurations forming at the centres of self-gravitating halos. These kiloparsec-scale soliton cores offer one possible solution to the cusp–core problem of CDM. Numerically, the Schrödinger–Poisson equations can, for example, be solved through adaptive spectral methods or through a reformulation into a hydrodynamics problem,

which can be solved with hydrodynamical discretization techniques, based on the Madelung formulation^{373,374}.

Alternative forms of dark energy

Cosmological simulations must include at least a cosmological constant to account for the accelerated expansion of the Universe. A wide range of alternative dark energy models have, however, been considered in the literature³⁷⁵ and a number of these have also been studied with simulations³⁷⁶.

Dynamical dark energy. The simplest extension in the dark energy sector is to assume a dark energy density that is time dependent, but still spatially homogeneous — at least on subhorizon scales. This behaviour can, for example, be obtained in scalar field models of dark energy³⁷⁶. Cosmic structure growth is then only affected via an altered background expansion. The only change required to perform cosmological simulations of such models is then to modify the calculation of the Hubble expansion rate in the numerical integration^{377,378}. As the growth function is different than in the Λ CDM model, extra care is also required when choosing the amplitude of matter density fluctuations in the initial conditions, for example, by taking into account at what redshift observational constraints on the amount of fluctuations are aimed to be matched. For example, models with a higher dark energy density at early times suppress structure growth and hence have lower amplitude fluctuations at redshift zero for the same scalar amplitude in the cosmic microwave background^{377,378}. Dynamical dark energy can have a surprisingly large impact on galaxy properties in simulations³⁷⁹. In practice, this results in degeneracies between cosmology and the feedback physics that is required to match observations.

Inhomogeneous dark energy. Models of dark energy that exhibit sizeable spatial fluctuations within the horizon represent the next level of complexity. For such models, and even more so, for the coupled dark energy models, a clear distinction between dark energy and modified gravity is often not possible as accelerations arising from spatial fluctuations in the dark energy field can also be interpreted as modifications to the laws of gravity. Relatively little simulation work has been done on models in which inhomogeneous dark energy interacts with matter only gravitationally, such as, for example, in the clustering dark energy scenario³⁸⁰.

Coupled dark energy. In the hope to alleviate the puzzle of the similar energy density of matter and dark energy at the present cosmic epoch, additional non-gravitational couplings between these sectors have been proposed³⁸¹. Such a coupling of dark energy to matter could be either universal, that is, involving all matter species, or non-universal, with dark energy, for example, coupling only to dark matter, but not to baryons. Models with a universal coupling typically require a screening mechanism that hides its effects in dense environments such as the Solar System, where experimental tests of gravity tightly constrain a direct coupling to baryons. In contrast, models with a coupling only to dark matter are

observationally much less constrained. In both cases, growing perturbations in the matter density field can naturally give rise to corresponding fluctuations in the coupled dark energy field. Coupled dark energy scenarios have been widely studied with simulations, either avoiding^{382,383} or including^{384,385} a treatment of the spatial fluctuations of dark energy. In the former case, the main effects of coupling terms are a time dependence of the gravitating particle mass of the coupled matter species, as well as a velocity-dependent friction term. Accounting for the spatial fluctuation additionally results in a fifth force proportional to the gradient of the dark energy field. These effects have, for example, been found to lower the concentrations and baryon fraction of halos³⁸³, thereby reducing potential tensions compared with a Λ CDM cosmology.

Alternative forms of gravity

Although general relativity has been tested to high precision within the Solar System, constraints on galactic and intergalactic scales are much weaker. Indeed, additional components that have so far not been directly observed, dark matter and dark energy, need to be added to allow a viable description of cosmology by general relativity. As an alternative, modifications of the laws of gravity have been proposed, which could make at least one of these components obsolete.

Modified gravity as an alternative to dark matter. Dark matter models successfully explain observations on many different scales, including the cosmic microwave background, the Lyman- α forest, the clustering of galaxies, and the internal dynamics of galaxies and galaxy clusters. Most work aimed at replacing the role of dark matter by a modification of the laws of gravity has focused only on a subset of these areas. For example, modified Newtonian dynamics^{386,387}, a change in Newton's second law at small acceleration values ($F = m\mu(|\mathbf{a}|/a_0)\mathbf{a}$, with $a_0 \sim 10^{-10} \text{ m s}^{-2}$ and $\mu(x) \rightarrow 1$ for $x \gg 1$ and $\mu(x) \rightarrow x$ for $x \ll 1$), where a is the acceleration, F denotes the force and μ is an interpolation function, or alternatively a change in Poisson's equation of Newtonian gravity ($\nabla \cdot (\mu(|\mathbf{a}|/a_0)\mathbf{a}) = 4\pi\rho$), has been proposed to account for the flat rotation curves of galaxies at large radii. Since this modified Poisson's equation is nonlinear, gravity algorithms that are based on the principle of linear force superposition, such as direct summation, tree and Fourier transform-based schemes, are not suitable to simulate these types of models. Simulations have therefore been performed with the multigrid method with the full approximation scheme²⁴. The nonlinear partial differential equation is then discretized on a grid with a finite difference representation of the differential operator and iteratively solved using Gauss-Seidel relaxation. Since modified Newtonian dynamics is not a relativistic theory, relativistic extensions of it have also been proposed, for example, tensor-vector-scalar gravity (TeVeS)^{388,389}. In this case, gravity is mediated by a tensor (metric), vector and scalar field. However, these models have not yet been widely studied in full cosmological simulations. Models without a dark matter component, such as modified Newtonian

dynamics, also naturally account for the tight observed relation between the gravitational acceleration inferred from galaxy rotation curves and that expected from the observed baryonic mass^{390,391}. However, galaxy formation simulations within the Λ CDM framework can also produce a sufficiently tight relation^{392–394}.

Modified gravity as an alternative to dark energy. Dark energy has only been observed through its impact on the background expansion of the Universe. Replacing dark energy with a modification to the laws of gravity is, compared with replacing dark matter, easier. In fact, a cosmological constant in the Einstein field equations can also be interpreted as modified gravity rather than an unexpectedly small zero-point energy of a quantum field. In the literature, a wide range of much more sophisticated modified gravity theories have been considered. Although many of these theories can account for the observed accelerated expansion of the Universe, Occam's razor would typically disfavour them compared with a cosmological constant in the absence of observational evidence beyond the observed background expansion. Cosmological simulations have been widely used to investigate the observational signatures of such extended gravity models to guide observational searches for potential modifications of gravity over a wide range of scales. Many modified gravity models that exhibit interesting behaviour on, for example, galactic and intergalactic scales have been designed such that they approach general relativity in dense environments such as the Solar System to avoid violating experimental constraints. Such screening mechanisms typically involve nonlinear partial differential equations, which renders them numerically challenging and requires tailored techniques³⁹⁵. Most schemes resort to the multigrid method with the full approximation scheme²⁴, for example, used on an adaptively refining mesh^{396–398}. With such methods, cosmological simulations have been carried out for a number of screened modified gravity models, including Chameleon- $f(R)$, Dvali–Gabadadze–Porrati (DGP), symmetron, dilaton and Galileon gravity^{399–401}. Most such studies focused on collisionless simulations. Semi-analytical galaxy formation models combined with Chameleon- $f(R)$ gravity demonstrated that the gravity modification effects on basic properties such as galaxy stellar mass functions and cosmic star formation rate densities are rather small and comparable to the uncertainties of the semi-analytical models⁴⁰². Clustering signals and relative velocities of halo pairs can, however, change notably^{402,403}. Post-processing Λ CDM galaxy formation simulations with a modified gravity solver suggests that there should be characteristic changes in the internal kinematics of galaxies, such as features in their rotation curves near the screening threshold⁴⁰⁴, which can also result in degeneracies with the core–cusp problem⁴⁰⁵. Fully self-consistent simulation studies of galaxy formation in such screened modified gravity models have only started very recently⁴⁰⁶. Such simulations should in principle also take into account effects that modified gravity has on stellar physics⁴⁰⁷.

Outlook

Cosmological simulations of galaxy formation play a crucial role in our understanding of galaxy formation. In particular, recent years have seen enormous progress on two fronts: large-volume simulations modelling large samples of galaxies and zoom simulations with refined galaxy formation models that resolve the physical processes in more detail. Modern galaxy formation simulations now reproduce numerous observational results and create virtual universes that are, to first order, nearly identical to the real Universe. At the same time, these simulations are also used to explore alternative cosmological models with modifications to the nature of dark matter, dark energy and gravity. This progress in the field of galaxy formation simulations has mostly been driven by a better understanding of galaxy formation physics, refined numerical methods and the steady growth of computing power.

Cosmological simulations of galaxy formation use a variety of different numerical methods and different implementations of galaxy formation physics. Despite these differences, such simulations have now converged on a wide range of predictions for the evolution of galaxies. It therefore seems that the basic physical mechanisms that shape the galaxy population have been identified, and that their current modelling is sufficient to produce realistic galaxy populations. However, these physical processes are implemented through still rather crude subresolution models. Subresolution models aim to capture the relevant physics through an effective description. In fact, cosmological simulations will always have to rely on these subresolution models since truly ab initio cosmological simulations of galaxy formation are and will remain impossible. One danger associated with the application of subresolution models is the belief that the reproduction of large amounts of observational data automatically implies a correct and physically plausible effective model and therefore detailed understanding of galaxy formation. This is problematic since subresolution models contain per construction a certain number of adjustable and degenerate parameters, and, at the same time, do not really capture the detailed physics at play, but only provide an effective coarse description. Caution is therefore required to not over-interpret some of the recent successes generated by these models.

One of the next goals of computational galaxy formation is to understand which detailed physical processes drive the outcomes of effective physical models. For example, many simulations use rather crude and incomplete models for the generation of galactic outflows without a detailed modelling of the driving process. Future simulations should aim at understanding these processes in more detail to illuminate the true physical processes at work going beyond the crude effective models to gain more fundamental insights. This will also lead to a better understanding of what physics actually drives the overall behaviour of currently existing coarse-grained effective subresolution models. While constructing new models and simulations, it is important to keep in mind that the major goal of simulations is not primarily to fit observed data, but rather to gain insights into galaxy formation physics. Advances in this direction more often benefit

from failures of certain ideas or models, rather than a perfect reproduction of observational data that is to some degree subject to the calibration of free model parameters and the coarse-grained nature of the employed models. Another frontier of cosmological galaxy formation simulations is the desire to provide large-volume simulations that match the statistical sample sizes of upcoming large observational surveys. This requires very

large-volume simulations with well-understood sub-resolution models. The development and better understanding of refined subresolution models, the desire to achieve higher numerical resolution and simulations with larger volumes represent the main challenges of cosmological simulations of the next decade.

Published online 8 January 2020

1. Somerville, R. S. & Davé, R. Physical models of galaxy formation in a cosmological framework. *Annu. Rev. Astron. Astrophys.* **53**, 51–113 (2015).
2. Naab, T. & Ostriker, J. P. Theoretical challenges in galaxy formation. *Annu. Rev. Astron. Astrophys.* **55**, 59–109 (2017).
3. Planck Collaboration et al. Planck 2015 results. XIII. Cosmological parameters. *Astron. Astrophys.* **594**, A13 (2016).
4. Seljak, U. & Zaldarriaga, M. A line-of-sight integration approach to cosmic microwave background anisotropies. *Astrophys. J.* **469**, 437 (1996).
5. Peacock, J. A. The evolution of galaxy clustering. *Mon. Not. R. Astron. Soc.* **284**, 885–898 (1997).
6. Eisenstein, D. J. & Hu, W. Baryonic features in the matter transfer function. *Astrophys. J.* **496**, 605–614 (1998).
7. Eisenstein, D. J. & Hu, W. Power spectra for cold dark matter and its variants. *Astrophys. J.* **511**, 5–15 (1999).
8. Baugh, C. M., Gaztanaga, E. & Efstathiou, G. A comparison of the evolution of density fields in perturbation theory and numerical simulations — II. Counts-in-cells analysis. *Mon. Not. R. Astron. Soc.* **274**, 1049–1070 (1995).
9. White, S. D. M. in *Cosmology and Large Scale Structure* (eds Schaeffer, R. et al.) 349–430 (Elsevier Science, 1996).
10. Zel'dovich, Y. B. Gravitational instability: an approximate theory for large density perturbations. *Astron. Astrophys.* **5**, 84–89 (1970).
11. Bertschinger, E. Multiscale Gaussian random fields and their application to cosmological simulations. *Astrophys. J. Suppl.* **137**, 1–20 (2001).
12. Jenkins, A. Second-order Lagrangian perturbation theory initial conditions for resimulations. *Mon. Not. R. Astron. Soc.* **403**, 1859–1872 (2010).
13. Hahn, O. & Abel, T. Multi-scale initial conditions for cosmological simulations. *Mon. Not. R. Astron. Soc.* **415**, 2101–2121 (2011).
14. Garrison, L. H., Eisenstein, D. J., Ferrer, D., Metchnik, M. V. & Pinto, P. A. Improving initial conditions for cosmological N -body simulations. *Mon. Not. R. Astron. Soc.* **461**, 4125–4145 (2016).
15. Hoffman, Y. & Ribak, E. Constrained realizations of Gaussian fields — a simple algorithm. *Astrophys. J. Lett.* **380**, L5–L8 (1991).
16. Salmon, J. Generation of correlated and constrained Gaussian stochastic processes for N -body simulations. *Astrophys. J.* **460**, 59 (1996).
17. Price, D. J. & Monaghan, J. J. An energy-conserving formalism for adaptive gravitational force softening in smoothed particle hydrodynamics and N -body codes. *Mon. Not. R. Astron. Soc.* **374**, 1347–1358 (2007).
18. Barnes, J. & Hut, P. A hierarchical $O(N \log N)$ force-calculation algorithm. *Nature* **324**, 446–449 (1986).
19. Dehnen, W. A very fast and momentum-conserving tree code. *Astrophys. J. Lett.* **536**, L59–L42 (2000).
20. Greengard, L. & Rokhlin, V. A fast algorithm for particle simulations. *J. Comput. Phys.* **73**, 325–348 (1987).
21. Hernquist, L., Bouchet, F. R. & Suto, Y. Application of the Ewald method to cosmological N -body simulations. *Astrophys. J. Suppl.* **75**, 231–240 (1991).
22. Ewald, P. Die Berechnung optischer und elektrostatischer Gitterpotentiale. *Ann. der Phys.* **369**, 253–287 (1921).
23. Hockney, R. W. & Eastwood, J. W. *Computer Simulation Using Particles* (McGraw-Hill, 1981).
24. Brandt, A. Multi-level adaptive solutions to boundary-value problems. *Math. Comput.* **31**, 333–390 (1977).
25. Efstathiou, G., Davis, M., White, S. D. M. & Frenk, C. S. Numerical techniques for large cosmological N -body simulations. *Astrophys. J. Suppl.* **57**, 241–260 (1985).
26. Bode, P. & Ostriker, J. P. Tree particle-mesh: an adaptive, efficient, and parallel code for collisionless cosmological simulation. *Astrophys. J. Suppl.* **145**, 1–13 (2003).
27. Kravtsov, A. V., Klypin, A. A. & Khokhlov, A. M. Adaptive refinement tree: a new high-resolution N -body code for cosmological simulations. *Astrophys. J. Suppl.* **111**, 73–94 (1997).
28. Wang, J. & White, S. D. M. Discreteness effects in simulations of hot/warm dark matter. *Mon. Not. R. Astron. Soc.* **380**, 93–103 (2007).
29. Widrow, L. M. & Kaiser, N. Using the Schrödinger equation to simulate collisionless matter. *Astrophys. J. Lett.* **416**, L71 (1993).
30. Schaller, M., Becker, C., Ruchayskiy, O., Boyarsky, A. & Shaposhnikov, M. A new framework for numerical simulations of structure formation. *Mon. Not. R. Astron. Soc.* **442**, 3073–3095 (2014).
31. Uhlemann, C., Kopp, M. & Haugg, T. Schrödinger method as N -body double and UV completion of dust. *Phys. Rev. D* **90**, 023517 (2014).
32. Colombi, S. & Tormen, G. Vlasov-Poisson in 1D: waterbags. *Mon. Not. R. Astron. Soc.* **441**, 2414–2432 (2014).
33. Colombi, S. Vlasov-Poisson in 1D for initially cold systems: post-collapse Lagrangian perturbation theory. *Mon. Not. R. Astron. Soc.* **446**, 2902–2920 (2015).
34. Vogelsberger, M., White, S. D. M., Helmi, A. & Springel, V. The fine-grained phase-space structure of cold dark matter haloes. *Mon. Not. R. Astron. Soc.* **385**, 236–254 (2008).
35. Vogelsberger, M. & White, S. D. M. Streams and caustics: the fine-grained structure of cold dark matter haloes. *Mon. Not. R. Astron. Soc.* **413**, 1419–1438 (2011).
36. Hahn, O., Abel, T. & Kaelher, R. A new approach to simulating collisionless dark matter fluids. *Mon. Not. R. Astron. Soc.* **434**, 1171–1191 (2013).
37. Yoshikawa, K., Yoshida, N. & Umemura, M. Direct integration of the collisionless Boltzmann equation in six-dimensional phase space: self-gravitating systems. *Astrophys. J.* **762**, 116 (2013).
38. Press, W. H. & Schechter, P. Formation of galaxies and clusters of galaxies by self-similar gravitational condensation. *Astrophys. J.* **187**, 425–438 (1974).
39. White, S. D. M. The dynamics of rich clusters of galaxies. *Mon. Not. R. Astron. Soc.* **177**, 717–733 (1976).
40. Aarseth, S. J., Gott, J. R. III & Turner, E. L. N -body simulations of galaxy clustering. I — Initial conditions and galaxy collapse times. *Astrophys. J.* **228**, 664–683 (1979).
41. Efstathiou, G. The clustering of galaxies and its dependence upon Omega. *Mon. Not. R. Astron. Soc.* **187**, 117–127 (1979).
42. Skillman, S. W. et al. Dark sky simulations: early data release. Preprint at [arXiv](https://arxiv.org/abs/1407.2600) <https://arxiv.org/abs/1407.2600> (2014).
43. Gnedin, O. Y., Kravtsov, A. V., Klypin, A. A. & Nagai, D. Response of dark matter halos to condensation of baryons: cosmological simulations and improved adiabatic contraction model. *Astrophys. J.* **616**, 16–26 (2004).
44. Di Cintio, A. et al. The dependence of dark matter profiles on the stellar-to-halo mass ratio: a prediction for cusps versus cores. *Mon. Not. R. Astron. Soc.* **437**, 415–423 (2014).
45. Zhu, Q. et al. Baryonic impact on the dark matter distribution in Milky Way-sized galaxies and their satellites. *Mon. Not. R. Astron. Soc.* **458**, 1559–1580 (2016).
46. Benítez-Llambay, A., Frenk, C. S., Ludlow, A. D. & Navarro, J. F. Baryon-induced dark matter cores in the EAGLE simulations. *Mon. Not. R. Astron. Soc.* **488**, 2387–2404 (2019).
47. Bose, S. et al. No cores in dark matter-dominated dwarf galaxies with bursty star formation histories. *Mon. Not. R. Astron. Soc.* **486**, 4790–4804 (2019).
48. Katz, H. et al. Stellar feedback and the energy budget of late-type galaxies: missing baryons and core creation. *Mon. Not. R. Astron. Soc.* **480**, 4287–4301 (2018).
49. Read, J. I., Walker, M. G. & Steger, P. Dark matter heats up in dwarf galaxies. *Mon. Not. R. Astron. Soc.* **484**, 1401–1420 (2019).
50. Diemer, B. & Kravtsov, A. V. Dependence of the outer density profiles of halos on their mass accretion rate. *Astrophys. J.* **789**, 1 (2014).
51. More, S., Diemer, B. & Kravtsov, A. V. The splashback radius as a physical halo boundary and the growth of halo mass. *Astrophys. J.* **810**, 36 (2015).
52. Diemer, B., More, S. & Kravtsov, A. V. The pseudo-evolution of halo mass. *Astrophys. J.* **766**, 25 (2013).
53. Davis, M., Efstathiou, G., Frenk, C. S. & White, S. D. M. The evolution of large-scale structure in a universe dominated by cold dark matter. *Astrophys. J.* **292**, 371–394 (1985).
54. Springel, V., White, S. D. M., Tormen, G. & Kauffmann, G. Populating a cluster of galaxies — I. Results at $z=0$. *Mon. Not. R. Astron. Soc.* **328**, 726–750 (2001).
55. Behroozi, P. S., Wechsler, R. H. & Wu, H.-Y. The ROCKSTAR phase-space temporal halo finder and the velocity offsets of cluster cores. *Astrophys. J.* **762**, 109 (2013).
56. Bond, J. R., Cole, S., Efstathiou, G. & Kaiser, N. Excursion set mass functions for hierarchical Gaussian fluctuations. *Astrophys. J.* **379**, 440–460 (1991).
57. Jenkins, A. et al. The mass function of dark matter haloes. *Mon. Not. R. Astron. Soc.* **321**, 372–384 (2001).
58. Sheth, R. K. & Tormen, G. An excursion set model of hierarchical clustering: ellipsoidal collapse and the moving barrier. *Mon. Not. R. Astron. Soc.* **329**, 61–75 (2002).
59. White, M. The mass function. *Astrophys. J. Suppl.* **143**, 241–255 (2002).
60. Reed, D. et al. Evolution of the mass function of dark matter haloes. *Mon. Not. R. Astron. Soc.* **346**, 565–572 (2003).
61. Warren, M. S., Abazajian, K., Holz, D. E. & Teodoro, L. Precision determination of the mass function of dark matter halos. *Astrophys. J.* **646**, 881–885 (2006).
62. Reed, D. S., Governato, F., Quinn, T., Stadel, J. & Lake, G. The age dependence of galaxy clustering. *Mon. Not. R. Astron. Soc.* **378**, 777–784 (2007).
63. Tinker, J. et al. Toward a halo mass function for precision cosmology: the limits of universality. *Astrophys. J.* **688**, 709–728 (2008).
64. Angulo, R. E., Hahn, O. & Abel, T. The warm dark matter halo mass function below the cut-off scale. *Mon. Not. R. Astron. Soc.* **434**, 3337–3347 (2013).
65. Schneider, A. Structure formation with suppressed small-scale perturbations. *Mon. Not. R. Astron. Soc.* **451**, 3117–3130 (2015).
66. Eke, V. R., Cole, S. & Frenk, C. S. Cluster evolution as a diagnostic for Omega. *Mon. Not. R. Astron. Soc.* **282**, 263–280 (1996).
67. Sheth, R. K., Mo, H. J. & Tormen, G. Ellipsoidal collapse and an improved model for the number and spatial distribution of dark matter haloes. *Mon. Not. R. Astron. Soc.* **323**, 1–12 (2001).
68. Angulo, R. E. et al. Scaling relations for galaxy clusters in the Millennium-XXL simulation. *Mon. Not. R. Astron. Soc.* **426**, 2046–2062 (2012).
69. Watson, W. A. et al. The halo mass function through the cosmic ages. *Mon. Not. R. Astron. Soc.* **433**, 1230–1245 (2013).
70. Heitmann, K. et al. The Q continuum simulation: harnessing the power of GPU accelerated supercomputers. *Astrophys. J. Suppl.* **219**, 34 (2015).
71. Bocquet, S., Saro, A., Dolag, K. & Mohr, J. J. Halo mass function: baryon impact, fitting formulae, and implications for cluster cosmology. *Mon. Not. R. Astron. Soc.* **456**, 2361–2373 (2016).
72. Springel, V., Frenk, C. S. & White, S. D. M. The large-scale structure of the Universe. *Nature* **440**, 1137–1144 (2006).
73. Springel, V. et al. First results from the IllustrisTNG simulations: matter and galaxy clustering. *Mon. Not. R. Astron. Soc.* **475**, 676–698 (2018).

74. Cooray, A. & Sheth, R. Halo models of large scale structure. *Phys. Rep.* **372**, 1–129 (2002).

75. Benson, A. J., Cole, S., Frenk, C. S., Baugh, C. M. & Lacey, C. G. The nature of galaxy bias and clustering. *Mon. Not. R. Astron. Soc.* **311**, 793–808 (2000).

76. Navarro, J. F., Frenk, C. S. & White, S. D. M. The structure of cold dark matter halos. *Astrophys. J.* **462**, 563 (1996).

77. Navarro, J. F., Frenk, C. S. & White, S. D. M. A universal density profile from hierarchical clustering. *Astrophys. J.* **490**, 493–508 (1997).

78. Moore, B. et al. Dark matter substructure within galactic halos. *Astrophys. J. Lett.* **524**, L19–L22 (1999).

79. Navarro, J. F. et al. The inner structure of Λ CDM haloes — III. Universality and asymptotic slopes. *Mon. Not. R. Astron. Soc.* **349**, 1039–1051 (2004).

80. Einasto, J. On the construction of a composite model for the galaxy and on the determination of the system of galactic parameters. *Trudy Astrofizicheskogo Inst. Alma-Ata 5*, 87–100 (1965).

81. Ludlow, A. D. et al. The mass–concentration–redshift relation of cold dark matter haloes. *Mon. Not. R. Astron. Soc.* **441**, 378–388 (2014).

82. Ludlow, A. D. et al. The mass–concentration–redshift relation of cold and warm dark matter haloes. *Mon. Not. R. Astron. Soc.* **460**, 1214–1232 (2016).

83. Klypin, A., Yepes, G., Gottlöber, S., Prada, F. & Heß, S. MultiDark simulations: the story of dark matter halo concentrations and density profiles. *Mon. Not. R. Astron. Soc.* **457**, 4340–4359 (2016).

84. Jing, Y. P. Intrinsic correlation of halo ellipticity and its implications for large-scale weak lensing surveys. *Mon. Not. R. Astron. Soc.* **335**, L89–L93 (2002).

85. Allgood, B. et al. The shape of dark matter haloes: dependence on mass, redshift, radius and formation. *Mon. Not. R. Astron. Soc.* **367**, 1781–1796 (2006).

86. Bett, P. et al. The spin and shape of dark matter haloes in the Millennium simulation of a Λ cold dark matter universe. *Mon. Not. R. Astron. Soc.* **376**, 215–232 (2007).

87. Diemand, J., Kuhlen, M. & Madau, P. Formation and evolution of galaxy dark matter halos and their substructure. *Astrophys. J.* **667**, 859–877 (2007).

88. Navarro, J. F. et al. The diversity and similarity of simulated cold dark matter haloes. *Mon. Not. R. Astron. Soc.* **402**, 21–34 (2010).

89. Bertschinger, E. Self-similar secondary infall and accretion in an Einstein–de Sitter universe. *Astrophys. J. Suppl.* **58**, 39–65 (1985).

90. Ghigna, S. et al. Dark matter haloes within clusters. *Mon. Not. R. Astron. Soc.* **300**, 146–162 (1998).

91. Springel, V. et al. The Aquarius Project: the subhaloes of galactic haloes. *Mon. Not. R. Astron. Soc.* **391**, 1685–1711 (2008).

92. Gao, L. et al. The Phoenix Project: the dark side of rich galaxy clusters. *Mon. Not. R. Astron. Soc.* **425**, 2169–2186 (2012).

93. Springel, V. et al. Prospects for detecting supersymmetric dark matter in the Galactic halo. *Nature* **456**, 73–76 (2008).

94. Gao, L., White, S. D. M., Jenkins, A., Stoehr, F. & Springel, V. The subhalo populations of Λ CDM dark haloes. *Mon. Not. R. Astron. Soc.* **355**, 819–834 (2004).

95. Colella, P. & Woodward, P. R. The piecewise parabolic method (PPM) for gas-dynamical simulations. *J. Comput. Phys.* **54**, 174–201 (1984).

96. Woodward, P. R. in *NATO Advanced Science Institutes (ASI) Series* Vol. 188 [eds Winkler, K.-H. A. & Norman, M. L.] 245 (Kluwer Academic, 1986).

97. Berger, M. J. & Oliger, J. Adaptive mesh refinement for hyperbolic partial differential equations. *J. Comput. Phys.* **53**, 484–512 (1984).

98. Berger, M. J. & Colella, P. Local adaptive mesh refinement for shock hydrodynamics. *J. Comput. Phys.* **82**, 64–84 (1989).

99. Klein, R. I., McKee, C. F. & Colella, P. On the hydrodynamic interaction of shock waves with interstellar clouds. I: Nonradiative shocks in small clouds. *Astrophys. J.* **420**, 213–236 (1994).

100. Bryan, G. L. & Norman, M. L. Simulating X-ray clusters with adaptive mesh refinement. Preprint at *arXiv* <https://arxiv.org/abs/astro-ph/9710186> (1995).

101. Cockburn, B., Lin, S.-Y. & Shu, C.-W. TVB Runge–Kutta local projection discontinuous Galerkin finite element method for conservation laws III: one-dimensional systems. *J. Comput. Phys.* **84**, 90–113 (1989).

102. Mocz, P., Vogelsberger, M., Sijacki, D., Pakmor, R. & Hernquist, L. A discontinuous Galerkin method for solving the fluid and magnetohydrodynamic equations in astrophysical simulations. *Mon. Not. R. Astron. Soc.* **437**, 397–414 (2014).

103. Guillet, T., Pakmor, R., Springel, V., Chandrashekar, P. & Klingenberg, C. High-order magnetohydrodynamics for astrophysics with an adaptive mesh refinement discontinuous galerkin scheme. *Mon. Not. R. Astron. Soc.* **485**, 4209–4246 (2019).

104. Lucy, L. B. A numerical approach to the testing of the fission hypothesis. *Astron. J.* **82**, 1013–1024 (1977).

105. Gingold, R. A. & Monaghan, J. J. Smoothed particle hydrodynamics — theory and application to non-spherical stars. *Mon. Not. R. Astron. Soc.* **181**, 375–389 (1977).

106. Springel, V. Smoothed particle hydrodynamics in astrophysics. *Annu. Rev. Astron. Astrophys.* **48**, 391–430 (2010).

107. Price, D. J. Smoothed particle hydrodynamics and magnetohydrodynamics. *J. Comput. Phys.* **231**, 759–794 (2012).

108. Read, J. I. & Hayfield, T. SPHS: smoothed particle hydrodynamics with a higher order dissipation switch. *Mon. Not. R. Astron. Soc.* **422**, 3037–3055 (2012).

109. Hopkins, P. F. A general class of Lagrangian smoothed particle hydrodynamics methods and implications for fluid mixing problems. *Mon. Not. R. Astron. Soc.* **428**, 2840–2856 (2013).

110. Keller, B. W., Wadsley, J., Benincasa, S. M. & Couchman, H. M. P. A superbubble feedback model for galaxy simulations. *Mon. Not. R. Astron. Soc.* **442**, 3013–3025 (2014).

111. Schaye, J. et al. The EAGLE project: simulating the evolution and assembly of galaxies and their environments. *Mon. Not. R. Astron. Soc.* **446**, 521–554 (2015).

112. Wang, L. et al. NIHAO project — I. Reproducing the inefficiency of galaxy formation across cosmic time with a large sample of cosmological hydrodynamical simulations. *Mon. Not. R. Astron. Soc.* **454**, 83–94 (2015).

113. Barnes, D. J. et al. The Cluster-EAGLE project: global properties of simulated clusters with resolved galaxies. *Mon. Not. R. Astron. Soc.* **471**, 1088–1106 (2017).

114. Gnedin, N. Y. Softened Lagrangian hydrodynamics for cosmology. *Astrophys. J. Suppl.* **97**, 231–257 (1995).

115. Pen, U.-L. A high-resolution adaptive moving mesh hydrodynamic algorithm. *Astrophys. J. Suppl.* **115**, 19–34 (1998).

116. Springel, V. *E pur si muove*: Galilean-invariant cosmological hydrodynamical simulations on a moving mesh. *Mon. Not. R. Astron. Soc.* **401**, 791–851 (2010).

117. Duffell, P. C. & MacFadyen, A. I. TESS: a relativistic hydrodynamics code on a moving Voronoi mesh. *Astrophys. J. Suppl.* **197**, 15 (2011).

118. Vandebroucke, B. & De Rijcke, S. The moving mesh code SHADOWFAX. *Astron. Comput.* **16**, 109–130 (2016).

119. Hopkins, P. F. A new class of accurate, mesh-free hydrodynamic simulation methods. *Mon. Not. R. Astron. Soc.* **450**, 53–110 (2015).

120. Sutherland, R. S. & Dopita, M. A. Cooling functions for low-density astrophysical plasmas. *Astrophys. J. Suppl.* **88**, 253–327 (1993).

121. Wiersma, R. P. C., Schaye, J. & Smith, B. D. The effect of photoionization on the cooling rates of enriched, astrophysical plasmas. *Mon. Not. R. Astron. Soc.* **393**, 99–107 (2009).

122. Haardt, F. & Madau, P. Radiative transfer in a clumpy universe. IV. new synthesis models of the cosmic UV/X-ray background. *Astrophys. J.* **746**, 125 (2012).

123. Tielens, A. G. G. M. *The Physics and Chemistry of the Interstellar Medium* (Cambridge Univ. Press, 2010).

124. Springel, V. & Hernquist, L. Cosmological smoothed particle hydrodynamics simulations: a hybrid multiphase model for star formation. *Mon. Not. R. Astron. Soc.* **339**, 289–311 (2003).

125. Agertz, O., Teyssier, R. & Moore, B. The formation of disc galaxies in a Λ CDM universe. *Mon. Not. R. Astron. Soc.* **410**, 1391–1408 (2011).

126. Dalla Vecchia, C. & Schaye, J. Simulating galactic outflows with thermal supernova feedback. *Mon. Not. R. Astron. Soc.* **426**, 140–158 (2012).

127. Hopkins, P. F., Quataert, E. & Murray, N. The structure of the interstellar medium of star-forming galaxies. *Mon. Not. R. Astron. Soc.* **421**, 3488–3521 (2012).

128. Agertz, O., Kravtsov, A. V., Leitner, S. N. & Gnedin, N. Y. Toward a complete accounting of energy and momentum from stellar feedback in galaxy formation simulations. *Astrophys. J.* **770**, 25 (2013).

129. Rosdahl, J., Schaye, J., Teyssier, R. & Agertz, O. Galaxies that shine: radiation-hydrodynamical simulations of disc galaxies. *Mon. Not. R. Astron. Soc.* **451**, 34–58 (2015).

130. Emerick, A., Bryan, G. L. & Mac Low, M.-M. Simulating an isolated dwarf galaxy with multichannel feedback and chemical yields from individual stars. *Mon. Not. R. Astron. Soc.* **482**, 1304–1329 (2019).

131. Krumholz, M. R. & Gnedin, N. Y. A comparison of methods for determining the molecular content of model galaxies. *Astrophys. J.* **729**, 36 (2011).

132. Bigiel, F. et al. A constant molecular gas depletion time in nearby disk galaxies. *Astrophys. J. Lett.* **730**, L13 (2011).

133. Krumholz, M. R., Dekel, A. & McKee, C. F. A universal, local star formation law in galactic clouds, nearby galaxies, high-redshift disks, and starbursts. *Astrophys. J.* **745**, 69 (2012).

134. Hopkins, P. F. et al. Galaxies on FIRE (Feedback in Realistic Environments): stellar feedback explains cosmologically inefficient star formation. *Mon. Not. R. Astron. Soc.* **445**, 581–603 (2014).

135. Hopkins, P. F. et al. FIRE-2 simulations: physics versus numerics in galaxy formation. *Mon. Not. R. Astron. Soc.* **480**, 800–863 (2018).

136. Stinson, G. et al. Star formation and feedback in smoothed particle hydrodynamic simulations — I. Isolated galaxies. *Mon. Not. R. Astron. Soc.* **373**, 1074–1090 (2006).

137. Teyssier, R., Pontzen, A., Dubois, Y. & Read, J. I. Cusp–core transformations in dwarf galaxies: observational predictions. *Mon. Not. R. Astron. Soc.* **429**, 3068–3078 (2013).

138. Vogelsberger, M. et al. Properties of galaxies reproduced by a hydrodynamic simulation. *Nature* **509**, 177–182 (2014).

139. Pillepich, A. et al. Simulating galaxy formation with the IllustrisTNG model. *Mon. Not. R. Astron. Soc.* **473**, 4077–4106 (2018).

140. Semenov, V. A., Kravtsov, A. V. & Gnedin, N. Y. The physical origin of long gas depletion times in galaxies. *Astrophys. J.* **845**, 133 (2017).

141. Trebitsch, M., Blaizot, J., Rosdahl, J., Devriendt, J. & Slyz, A. Fluctuating feedback-regulated escape fraction of ionizing radiation in low-mass, high-redshift galaxies. *Mon. Not. R. Astron. Soc.* **470**, 224–239 (2017).

142. Rosdahl, J. et al. The SPHINX cosmological simulations of the first billion years: the impact of binary stars on reionization. *Mon. Not. R. Astron. Soc.* **479**, 994–1016 (2018).

143. Gnedin, N. Y. & Kravtsov, A. V. Environmental dependence of the Kennicutt–Schmidt relation in galaxies. *Astrophys. J.* **728**, 88 (2011).

144. Christensen, C. et al. Implementing molecular hydrogen hydrodynamic simulations of galaxy formation. *Mon. Not. R. Astron. Soc.* **425**, 3058–3076 (2012).

145. Feldmann, R., Gnedin, N. Y. & Kravtsov, A. V. The X-factor in galaxies. II. The molecular-hydrogen–star-formation relation. *Astrophys. J.* **758**, 127 (2012).

146. Kuhlen, M., Krumholz, M. R., Madau, P., Smith, B. D. & Wise, J. Dwarf galaxy formation with H_2 -regulated star formation. *Astrophys. J.* **749**, 36 (2012).

147. Monaco, P., Murante, G., Borgani, S. & Dolag, K. Schmidt–Kennicutt relations in SPH simulations of disc galaxies with effective thermal feedback from supernovae. *Mon. Not. R. Astron. Soc.* **421**, 2485–2497 (2012).

148. Li, H. et al. Star cluster formation in cosmological simulations. I. Properties of young clusters. *Astrophys. J.* **834**, 69 (2017).

149. Wiersma, R. P. C., Schaye, J., Theuns, T., Dalla Vecchia, C. & Tornatore, L. Chemical enrichment in cosmological, smoothed particle hydrodynamics simulations. *Mon. Not. R. Astron. Soc.* **399**, 574–600 (2009).

150. Vogelsberger, M. et al. A model for cosmological simulations of galaxy formation physics. *Mon. Not. R. Astron. Soc.* **436**, 3031–3067 (2013).

151. Naiman, J. P. et al. First results from the IllustrisTNG simulations: a tale of two elements — chemical evolution of magnesium and europium. *Mon. Not. R. Astron. Soc.* **477**, 1206–1224 (2018).

152. Oppenheimer, B. D. et al. Feedback and recycled wind accretion: assembling the $z=0$ galaxy mass function. *Mon. Not. R. Astron. Soc.* **406**, 2325–2338 (2010).

153. Stinson, G. S. et al. Making galaxies in a cosmological context: the need for early stellar feedback. *Mon. Not. R. Astron. Soc.* **428**, 129–140 (2013).

154. Smith, M. C., Sijacki, D. & Shen, S. Cosmological simulations of dwarfs: the need for ISM physics

beyond SN feedback alone. *Mon. Not. R. Astron. Soc.* **485**, 3317–3333 (2019).

155. Behroozi, P. S., Conroy, C. & Wechsler, R. H. A comprehensive analysis of uncertainties affecting the stellar mass–halo mass relation for $0 < z < 4$. *Astrophys. J.* **717**, 379–403 (2010).

156. Moster, B. P., Naab, T. & White, S. D. M. Galactic star formation and accretion histories from matching galaxies to dark matter haloes. *Mon. Not. R. Astron. Soc.* **428**, 3121–3138 (2013).

157. Muratov, A. L. et al. Gusty, gaseous flows of FIRE: galactic winds in cosmological simulations with explicit stellar feedback. *Mon. Not. R. Astron. Soc.* **454**, 2691–2713 (2015).

158. Gehren, T., Fried, J., Wehinger, P. A. & Wyckoff, S. Host galaxies of quasars and their association with galaxy clusters. *Astrophys. J.* **278**, 11–27 (1984).

159. Kormendy, J. & Richstone, D. Inward bound — the search for supermassive black holes in galactic nuclei. *Annu. Rev. Astron. Astrophys.* **33**, 581 (1995).

160. Filippenko, A. V. & Ho, L. C. A low-mass central black hole in the bulgeless Seyfert 1 galaxy NGC 4395. *Astrophys. J. Lett.* **588**, L13–L16 (2003).

161. Shields, J. C. et al. An accreting black hole in the nuclear star cluster of the bulgeless galaxy NGC 1042. *Astrophys. J.* **682**, 104–109 (2008).

162. Reines, A. E., Sivakoff, G. R., Johnson, K. E. & Brogan, C. L. An actively accreting massive black hole in the dwarf starburst galaxy Henize2-10. *Nature* **470**, 66–68 (2011).

163. Moran, E. C., Shahinyan, K., Sugarman, H. R., Vélez, D. O. & Eracleous, M. Black holes at the centers of nearby dwarf galaxies. *Astron. J.* **148**, 136 (2014).

164. Booth, C. M. & Schaye, J. Cosmological simulations of the growth of supermassive black holes and feedback from active galactic nuclei: method and tests. *Mon. Not. R. Astron. Soc.* **398**, 53–74 (2009).

165. Shlosman, I., Frank, J. & Begelman, M. C. Bars within bars — a mechanism for fuelling active galactic nuclei. *Nature* **338**, 45–47 (1989).

166. Hopkins, P. F. & Quataert, E. An analytic model of angular momentum transport by gravitational torques: from galaxies to massive black holes. *Mon. Not. R. Astron. Soc.* **415**, 1027–1050 (2011).

167. Bournaud, F. et al. Black hole growth and active galactic nuclei obscuration by instability-driven inflows in high-redshift disk galaxies fed by cold streams. *Astrophys. J. Lett.* **741**, L33 (2011).

168. Gabor, J. M. & Bournaud, F. Simulations of supermassive black hole growth in high-redshift disc galaxies. *Mon. Not. R. Astron. Soc.* **434**, 606–620 (2013).

169. Anglés-Alcázar, D., Özel, F. & Davé, R. Black hole–galaxy correlations without self-regulation. *Astrophys. J.* **770**, 5 (2013).

170. Anglés-Alcázar, D. et al. Black holes on FIRE: stellar feedback limits early feeding of galactic nuclei. *Mon. Not. R. Astron. Soc.* **472**, L109–L114 (2017).

171. Davé, R. et al. SIMBA: cosmological simulations with black hole growth and feedback. *Mon. Not. R. Astron. Soc.* **486**, 2827–2849 (2019).

172. Krolik, J. H. *Active Galactic Nuclei: From the Central Black Hole to the Galactic Environment* (Princeton Univ. Press, 1999).

173. Springel, V., Di Matteo, T. & Hernquist, L. Modelling feedback from stars and black holes in galaxy mergers. *Mon. Not. R. Astron. Soc.* **361**, 776–794 (2005).

174. Di Matteo, T., Springel, V. & Hernquist, L. Energy input from quasars regulates the growth and activity of black holes and their host galaxies. *Nature* **433**, 604–607 (2005).

175. Debuhr, J., Quataert, E., Ma, C.-P. & Hopkins, P. Self-regulated black hole growth via momentum deposition in galaxy merger simulations. *Mon. Not. R. Astron. Soc.* **406**, L55–L59 (2010).

176. Costa, T., Rosdahl, J., Sijacki, D. & Haehnelt, M. G. Driving gas shells with radiation pressure on dust in radiation–hydrodynamic simulations. *Mon. Not. R. Astron. Soc.* **473**, 4197–4219 (2018).

177. Barnes, D. J., Kannan, R., Vogelsberger, M. & Marinacci, F. Radiative AGN feedback on a moving mesh: the impact of the galactic disc and dust physics on outflow properties. Preprint at (2018).

178. Choi, E., Ostriker, J. P., Naab, T. & Johansson, P. H. Radiative and momentum-based mechanical active galactic nucleus feedback in a three-dimensional galaxy evolution code. *Astrophys. J.* **754**, 125 (2012).

179. Sijacki, D., Springel, V., Di Matteo, T. & Hernquist, L. A unified model for AGN feedback in cosmological simulations of structure formation. *Mon. Not. R. Astron. Soc.* **380**, 877–900 (2007).

180. Weinberger, R. et al. Simulating galaxy formation with black hole driven thermal and kinetic feedback. *Mon. Not. R. Astron. Soc.* **465**, 3291–3308 (2017).

181. Marinacci, F. & Vogelsberger, M. Effects of simulated cosmological magnetic fields on the galaxy population. *Mon. Not. R. Astron. Soc.* **456**, L69–L73 (2016).

182. Ferrière, K. M. The interstellar environment of our galaxy. *Rev. Mod. Phys.* **73**, 1031–1066 (2001).

183. Kotera, K. & Olinto, A. V. The astrophysics of ultrahigh-energy cosmic rays. *Annu. Rev. Astron. Astrophys.* **49**, 119–155 (2011).

184. Donnert, J., Dolag, K., Lesch, H. & Müller, E. Cluster magnetic fields from galactic outflows. *Mon. Not. R. Astron. Soc.* **392**, 1008–1021 (2009).

185. Marinacci, F. et al. First results from the IllustrisTNG simulations: radio haloes and magnetic fields. *Mon. Not. R. Astron. Soc.* **480**, 5113–5139 (2018).

186. Pakmor, R. et al. Magnetic field formation in the Milky Way like disc galaxies of the Auriga project. *Mon. Not. R. Astron. Soc.* **469**, 3185–3199 (2017).

187. Powell, K. G., Roe, P. L., Linde, T. J., Gombosi, T. I. & De Zeeuw, D. L. A solution-adaptive upwind scheme for ideal magnetohydrodynamics. *J. Comput. Phys.* **154**, 284–309 (1999).

188. Dedner, A. et al. Hyperbolic divergence cleaning for the MHD equations. *J. Comput. Phys.* **175**, 645–673 (2002).

189. Evans, C. R. & Hawley, J. F. Simulation of magnetohydrodynamic flows — a constrained transport method. *Astrophys. J.* **332**, 659–677 (1988).

190. Mocz, P. et al. A moving mesh unstaggered constrained transport scheme for magnetohydrodynamics. *Mon. Not. R. Astron. Soc.* **463**, 477–488 (2016).

191. Rosswog, S. & Price, D. MAGMA: a three-dimensional, Lagrangian magnetohydrodynamics code for merger applications. *Mon. Not. R. Astron. Soc.* **379**, 915–931 (2007).

192. Dolag, K. & Stasyszyn, F. An MHD GADGET for cosmological simulations. *Mon. Not. R. Astron. Soc.* **398**, 1678–1697 (2009).

193. Stone, J. M. & Norman, M. L. ZEUS-2D: a radiation magnetohydrodynamics code for astrophysical flows in two space dimensions. II. The magnetohydrodynamic algorithms and tests. *Astrophys. J. Suppl.* **80**, 791 (1992).

194. Londrillo, P. & del Zanna, L. On the divergence-free condition in Godunov-type schemes for ideal magnetohydrodynamics: the upwind constrained transport method. *J. Comput. Phys.* **195**, 17–48 (2004).

195. Fromang, S., Hennebelle, P. & Teyssier, R. A high order Godunov scheme with constrained transport and adaptive mesh refinement for astrophysical magnetohydrodynamics. *Astron. Astrophys.* **457**, 371–384 (2006).

196. Teyssier, R., Fromang, S. & Dormy, E. Kinematic dynamos using constrained transport with high order Godunov schemes and adaptive mesh refinement. *J. Comput. Phys.* **218**, 44–67 (2006).

197. Balsara, D. S. A two-dimensional HLLC Riemann solver for conservation laws: application to Euler and magnetohydrodynamic flows. *J. Comput. Phys.* **231**, 7476–7503 (2012).

198. Ferrière, K. Magnetic fields in galaxies: their origin and their impact on the interstellar medium. *Acta Astron. Sin.* **44**, 115–122 (2003).

199. Cox, D. P. The three-phase interstellar medium revisited. *Annu. Rev. Astron. Astrophys.* **43**, 337–385 (2005).

200. Field, G. B., Goldsmith, D. W. & Habing, H. J. Cosmic-ray heating of the interstellar gas. *Astrophys. J. Lett.* **155**, L149 (1969).

201. Wolfe, M. G., Hollenbach, D., McKee, C. F., Tielens, A. G. G. M. & Bakes, E. L. O. The neutral atomic phases of the interstellar medium. *Astrophys. J.* **443**, 152–168 (1995).

202. Uhlig, M. et al. Galactic winds driven by cosmic ray streaming. *Mon. Not. R. Astron. Soc.* **423**, 2374–2396 (2012).

203. Booth, C. M., Agertz, O., Kravtsov, A. V. & Gnedin, N. Y. Simulations of disk galaxies with cosmic ray driven galactic winds. *Astrophys. J. Lett.* **777**, L16 (2013).

204. Hanasz, M. et al. Cosmic rays can drive strong outflows from gas-rich high-redshift disk galaxies. *Astrophys. J. Lett.* **777**, L38 (2013).

205. Salem, M., Bryan, G. L. & Hummels, C. Cosmological simulations of galaxy formation with cosmic rays. *Astrophys. J. Lett.* **797**, L18 (2014).

206. Pakmor, R., Pfrommer, C., Simpson, C. M. & Springel, V. Galactic winds driven by isotropic and anisotropic cosmic-ray diffusion in disk galaxies. *Astrophys. J. Lett.* **824**, L30 (2016).

207. Simpson, C. M. et al. The role of cosmic-ray pressure in accelerating galactic outflows. *Astrophys. J. Lett.* **827**, L29 (2016).

208. Ruszkowski, M., Yang, H.-Y. K. & Zweibel, E. Global simulations of galactic winds including cosmic-ray streaming. *Astrophys. J.* **834**, 208 (2017).

209. Farber, R., Ruszkowski, M., Yang, H.-Y. K. & Zweibel, E. G. Impact of cosmic-ray transport on galactic winds. *Astrophys. J.* **856**, 112 (2018).

210. Girichidis, P., Naab, T., Hanasz, M. & Walch, S. Cooler and smoother — the impact of cosmic rays on the phase structure of galactic outflows. *Mon. Not. R. Astron. Soc.* **479**, 3042–3067 (2018).

211. Jacob, S., Pakmor, R., Simpson, C. M., Springel, V. & Pfrommer, C. The dependence of cosmic-ray-driven galactic winds on halo mass. *Mon. Not. R. Astron. Soc.* **475**, 570–584 (2018).

212. Pfrommer, C., Pakmor, R., Schaaf, K., Simpson, C. M. & Springel, V. Simulating cosmic ray physics on a moving mesh. *Mon. Not. R. Astron. Soc.* **465**, 4500–4529 (2017).

213. Sharma, P. & Hammett, G. W. Preserving monotonicity in anisotropic diffusion. *J. Comput. Phys.* **227**, 123–142 (2007).

214. Kannan, R., Springel, V., Pakmor, R., Marinacci, F. & Vogelsberger, M. Accurately simulating anisotropic thermal conduction on a moving mesh. *Mon. Not. R. Astron. Soc.* **458**, 410–424 (2016).

215. Butsky, I. S. & Quinn, T. R. The role of cosmic-ray transport in shaping the simulated circumgalactic medium. *Astrophys. J.* **868**, 108 (2018).

216. Sharma, P., Colella, P. & Martin, D. Numerical implementation of streaming down the gradient: application fluid modeling of cosmic rays and saturated conduction. *Siam J. Sci. Comput.* **32**, 3476–3494 (2009).

217. Jiang, Y.-F. & Oh, S. P. A new numerical scheme for cosmic-ray transport. *Astrophys. J.* **854**, 5 (2018).

218. Thomas, T. & Pfrommer, C. Cosmic-ray hydrodynamics: Alfvén-wave regulated transport of cosmic rays. *Mon. Not. R. Astron. Soc.* **485**, 2977–3008 (2019).

219. Gnedin, N. Y. & Kaurov, A. A. Cosmic reionization on computers. II. Reionization history and its back-reaction on early galaxies. *Astrophys. J.* **793**, 30 (2014).

220. Ocvirk, P. et al. Cosmic Dawn II (CoDa II): a new radiation-hydrodynamics simulation of the self-consistent coupling of galaxy formation and reionization. Preprint at (2018).

221. Wise, J. H., Abel, T., Turk, M. J., Norman, M. L. & Smith, B. D. The birth of a galaxy — II. The role of radiation pressure. *Mon. Not. R. Astron. Soc.* **427**, 311–326 (2012).

222. Gnedin, N. Y. & Abel, T. Multi-dimensional cosmological radiative transfer with a Variable Eddington Tensor formalism. *New Astron.* **6**, 437–455 (2001).

223. Gnedin, N. Y. On the proper use of the reduced speed of light approximation. *Astrophys. J.* **833**, 66 (2016).

224. Deparis, N., Aubert, D., Ocvirk, P., Chardin, J. & Lewis, J. Impact of the reduced speed of light approximation on ionization front velocities in cosmological simulations of the epoch of reionization. *Astron. Astrophys.* **622**, A142 (2019).

225. Ocvirk, P., Aubert, D., Chardin, J., Deparis, N. & Lewis, J. Impact of the reduced speed of light approximation on the post-overlap neutral hydrogen fraction in numerical simulations of the epoch of reionization. *Astron. Astrophys.* **626**, A77 (2019).

226. Mihalas, D. & Mihalas, B. W. *Foundations of Radiation Hydrodynamics* (Oxford Univ. Press, 1984).

227. Abel, T., Norman, M. L. & Madau, P. Photon-conserving radiative transfer around point sources in multidimensional numerical cosmology. *Astrophys. J.* **523**, 66–71 (1999).

228. Jaura, O., Glover, S. C. O., Klessen, R. S. & Paardekooper, J.-P. SPRAI: coupling of radiative feedback and primordial chemistry in moving mesh hydrodynamics. *Mon. Not. R. Astron. Soc.* **475**, 2822–2834 (2018).

229. Rijkhorst, E.-J., Plewa, T., Dubey, A. & Mellema, G. Hybrid characteristics: 3D radiative transfer for parallel adaptive mesh refinement hydrodynamics. *Astron. Astrophys.* **452**, 907–920 (2006).

230. Rosen, A. L., Krumholz, M. R., Oishi, J. S., Lee, A. T. & Klein, R. I. Hybrid Adaptive Ray-Moment Method (HARM): a highly parallel method for radiation hydrodynamics on adaptive grids. *J. Comput. Phys.* **330**, 924–942 (2017).

231. Whalen, D. & Norman, M. L. A multistep algorithm for the radiation hydrodynamical transport of cosmological ionization fronts and ionized flows. *Astrophys. J. Suppl.* **162**, 281–303 (2006).

232. Trac, H. & Cen, R. Radiative transfer simulations of cosmic reionization. I. Methodology and initial results. *Astrophys. J.* **671**, 1–13 (2007).

233. Pawlik, A. H. & Schaye, J. TRAPHIC — radiative transfer for smoothed particle hydrodynamics simulations. *Mon. Not. R. Astron. Soc.* **389**, 651–677 (2008).

234. Petkova, M. & Springel, V. A novel approach for accurate radiative transfer in cosmological hydrodynamic simulations. *Mon. Not. R. Astron. Soc.* **415**, 3731–3749 (2011).

235. Ciardi, B., Ferrara, A., Marri, S. & Raimondo, G. Cosmological reionization around the first stars: Monte Carlo radiative transfer. *Mon. Not. R. Astron. Soc.* **324**, 381–388 (2001).

236. Oxley, S. & Woolfson, M. M. Smoothed particle hydrodynamics with radiation transfer. *Mon. Not. R. Astron. Soc.* **343**, 900–912 (2003).

237. Tasitsiomi, A. Ly Radiative transfer in cosmological simulations and application to $z = 8$ Ly emitter. *Astrophys. J.* **645**, 792–813 (2006).

238. Semelin, B., Combes, F. & Baek, S. Lyman-alpha radiative transfer during the epoch of reionization: contribution to 21-cm signal fluctuations. *Astron. Astrophys.* **474**, 365–374 (2007).

239. Dullemond, C. P. et al. RADMC-3D: A Multi-purpose Radiative Transfer Tool (Astrophysics Source Code Library, 2012).

240. Smith, A. et al. The physics of Lyman escape from high-redshift galaxies. *Mon. Not. R. Astron. Soc.* **484**, 39–59 (2019).

241. Lucy, L. B. Improved Monte Carlo techniques for the spectral synthesis of supernovae. *Astron. Astrophys.* **345**, 211–220 (1999).

242. Gentile, N. A. Implicit Monte Carlo diffusion — an acceleration method for Monte Carlo time-dependent radiative transfer simulations. *J. Comput. Phys.* **172**, 543–571 (2001).

243. Densmore, J. D., Urbatsch, T. J., Evans, T. M. & Buksas, M. W. A hybrid transport-diffusion method for Monte Carlo radiative-transfer simulations. *J. Comput. Phys.* **222**, 485–503 (2007).

244. Smith, A., Tsang, B. T. H., Bromm, V. & Milosavljević, M. Discrete diffusion Lyman radiative transfer. *Mon. Not. R. Astron. Soc.* **479**, 2065–2078 (2018).

245. Levermore, C. D. Relating Eddington factors to flux limiters. *J. Quant. Spectrosc. Radiat. Transf.* **31**, 149–160 (1984).

246. González, M., Audit, E. & Huynh, P. HERACLES: a three-dimensional radiation hydrodynamics code. *Astron. Astrophys.* **464**, 429–435 (2007).

247. Rosdahl, J., Blaizot, J., Aubert, D., Stranex, T. & Teyssier, R. RAMSES-RT: radiation hydrodynamics in the cosmological context. *Mon. Not. R. Astron. Soc.* **436**, 2188–2231 (2013).

248. Kannan, R. et al. AREPO-RT: radiation hydrodynamics on a moving mesh. *Mon. Not. R. Astron. Soc.* **485**, 117–149 (2019).

249. Krumholz, M. R., Klein, R. I., McKee, C. F. & Bolstad, J. Equations and algorithms for mixed-frame flux-limited diffusion radiation hydrodynamics. *Astrophys. J.* **667**, 626–643 (2007).

250. Finlator, K., Özel, F. & Davé, R. A new moment method for continuum radiative transfer in cosmological re-ionization. *Mon. Not. R. Astron. Soc.* **393**, 1090–1106 (2009).

251. Petkova, M. & Springel, V. An implementation of radiative transfer in the cosmological simulation code GADGET. *Mon. Not. R. Astron. Soc.* **396**, 1383–1403 (2009).

252. Dubroca, B. & Feugeas, J. Etude théorique et numérique d'une hiérarchie de modèles aux moments pour le transfert radiatif. *C. R. Acad. Sci. Math.* **329**, 915–920 (1999).

253. Ripoll, J.-F., Dubroca, B. & Duffa, G. Modelling radiative mean absorption coefficients. *Combust. Theory Model.* **5**, 261–274 (2001).

254. McKinnon, R., Torrey, P. & Vogelsberger, M. Dust formation in Milky Way-like galaxies. *Mon. Not. R. Astron. Soc.* **457**, 3775–3800 (2016).

255. Aoyama, S. et al. Galaxy simulation with dust formation and destruction. *Mon. Not. R. Astron. Soc.* **466**, 105–121 (2017).

256. Hou, K.-C., Hirashita, H., Nagamine, K., Aoyama, S. & Shimizu, I. Evolution of dust extinction curves in galaxy simulation. *Mon. Not. R. Astron. Soc.* **469**, 870–885 (2017).

257. McKinnon, R., Torrey, P., Vogelsberger, M., Hayward, C. C. & Marinacci, F. Simulating the dust content of galaxies: successes and failures. *Mon. Not. R. Astron. Soc.* **468**, 1505–1521 (2017).

258. Aoyama, S., Hou, K.-C., Hirashita, H., Nagamine, K. & Shimizu, I. Cosmological simulation with dust formation and destruction. *Mon. Not. R. Astron. Soc.* **478**, 4905–4921 (2018).

259. McKinnon, R., Vogelsberger, M., Torrey, P., Marinacci, F. & Kannan, R. Simulating galactic dust grain evolution on a moving mesh. *Mon. Not. R. Astron. Soc.* **478**, 2851–2886 (2018).

260. Vogelsberger, M. et al. Dust in and around galaxies: dust in cluster environments and its impact on gas cooling. *Mon. Not. R. Astron. Soc.* **487**, 4870–4883 (2019).

261. Gjergo, E. et al. Dust evolution in galaxy cluster simulations. *Mon. Not. R. Astron. Soc.* **479**, 2588–2606 (2018).

262. Hou, K.-C., Aoyama, S., Hirashita, H., Nagamine, K. & Shimizu, I. Dust scaling relations in a cosmological simulation. *Mon. Not. R. Astron. Soc.* **485**, 1727–1744 (2019).

263. Ruszkowski, M., Lee, D., Brüggen, M., Parrish, I. & Oh, S. P. Cosmological magnetohydrodynamic simulations of cluster formation with anisotropic thermal conduction. *Astrophys. J.* **740**, 81 (2011).

264. Smith, B., O'Shea, B. W., Voit, G. M., Ventimiglia, D. & Skillman, S. W. Cosmological simulations of isotropic conduction in galaxy clusters. *Astrophys. J.* **778**, 152 (2013).

265. Arth, A., Dolag, K., Beck, A. M., Petkova, M. & Lesch, H. Anisotropic thermal conduction in galaxy clusters with MHD in Gadget. Preprint at (2014).

266. Yang, H.-Y. K. & Reynolds, C. S. Interplay among cooling, agn feedback, and anisotropic conduction in the cool cores of galaxy clusters. *Astrophys. J.* **818**, 181 (2016).

267. Kannan, R. et al. Increasing black hole feedback-induced quenching with anisotropic thermal conduction. *Astrophys. J. Lett.* **837**, L18 (2017).

268. Parrish, I. J., McCourt, M., Quataert, E. & Sharma, P. The effects of anisotropic viscosity on turbulence and heat transport in the intracluster medium. *Mon. Not. R. Astron. Soc.* **422**, 704–718 (2012).

269. Suzuki, K., Ogawa, T., Matsumoto, Y. & Matsumoto, R. Magnetohydrodynamic simulations of the formation of cold fronts in clusters of galaxies: effects of anisotropic viscosity. *Astrophys. J.* **768**, 175 (2013).

270. ZuHone, J. A., Kunz, M. W., Markevitch, M., Stone, J. M. & Biffi, V. The effect of anisotropic viscosity on cold fronts in galaxy clusters. *Astrophys. J.* **798**, 90 (2015).

271. Su, K.-Y. et al. Feedback first: the surprisingly weak effects of magnetic fields, viscosity, conduction and metal diffusion on sub-L* galaxy formation. *Mon. Not. R. Astron. Soc.* **471**, 144–166 (2017).

272. Balbus, S. A. Stability, instability, and “backward” transport in stratified fluids. *Astrophys. J.* **534**, 420–427 (2000).

273. Quataert, E. Buoyancy instabilities in weakly magnetized low-collimation plasmas. *Astrophys. J.* **673**, 758–762 (2008).

274. Barnes, D. J. et al. Enhancing AGN efficiency and cool-core formation with anisotropic thermal conduction. Preprint at (2018).

275. Torrey, P. et al. Synthetic galaxy images and spectra from the Illustris simulation. *Mon. Not. R. Astron. Soc.* **447**, 2753–2771 (2015).

276. Trayford, J. W. et al. Optical colours and spectral indices of $z = 0.1$ eagle galaxies with the 3D dust radiative transfer code skirt. *Mon. Not. R. Astron. Soc.* **470**, 771–799 (2017).

277. Hernquist, L., Katz, N., Weinberg, D. H. & Miralda-Escudé, J. The Lyman-alpha forest in the cold dark matter model. *Astrophys. J. Lett.* **457**, L51 (1996).

278. Katz, N. & Gunn, J. E. Dissipational galaxy formation. I — effects of gas dynamics. *Astrophys. J.* **377**, 365–381 (1991).

279. Navarro, J. F. & Benz, W. Dynamics of cooling gas in galactic dark halos. *Astrophys. J.* **380**, 320–329 (1991).

280. Katz, N. Dissipational galaxy formation. II — effects of star formation. *Astrophys. J.* **391**, 502–517 (1992).

281. Katz, N., Hernquist, L. & Weinberg, D. H. Galaxies and gas in a cold dark matter universe. *Astrophys. J. Lett.* **399**, L109–L112 (1992).

282. Navarro, J. F. & Steinmetz, M. The effects of a photoionizing ultraviolet background on the formation of disk galaxies. *Astrophys. J.* **478**, 13–28 (1997).

283. Navarro, J. F. & Steinmetz, M. Dark halo and disk galaxy scaling laws in hierarchical universes. *Astrophys. J.* **538**, 477–488 (2000).

284. Abadi, M. G., Navarro, J. F., Steinmetz, M. & Eke, V. R. Simulations of galaxy formation in a Λ cold dark matter universe. I. Dynamical and photometric properties of a simulated disk galaxy. *Astrophys. J.* **591**, 499–514 (2003).

285. Scannapieco, C., Tissera, P. B., White, S. D. M. & Springel, V. Effects of supernova feedback on the formation of galaxy discs. *Mon. Not. R. Astron. Soc.* **389**, 1137–1149 (2008).

286. Grand, R. J. J. et al. The Auriga Project: the properties and formation mechanisms of disc galaxies across cosmic time. *Mon. Not. R. Astron. Soc.* **467**, 179–207 (2017).

287. Kaviraj, S. et al. The Horizon-AGN simulation: evolution of galaxy properties over cosmic time. *Mon. Not. R. Astron. Soc.* **467**, 4739–4752 (2017).

288. Schechter, P. An analytic expression for the luminosity function for galaxies. *Astrophys. J.* **203**, 297–306 (1976).

289. Panter, B., Jimenez, R., Heavens, A. F. & Charlot, S. The star formation histories of galaxies in the Sloan Digital Sky Survey. *Mon. Not. R. Astron. Soc.* **378**, 1550–1564 (2007).

290. Pozzetti, L. et al. zCOSMOS — 10k-bright spectroscopic sample. The bimodality in the galaxy stellar mass function: exploring its evolution with redshift. *Astron. Astrophys.* **523**, A13 (2010).

291. Baldry, I. K. et al. Galaxy and mass assembly (GAMA): the galaxy stellar mass function at $z < 0.06$. *Mon. Not. R. Astron. Soc.* **421**, 621–634 (2012).

292. Ilbert, O. et al. Mass assembly in quiescent and star-forming galaxies since $z \simeq 4$ from UltraVISTA. *Astron. Astrophys.* **556**, A55 (2013).

293. Muzzin, A. et al. The evolution of the stellar mass functions of star-forming and quiescent galaxies to $z = 4$ from the COSMOS/UltraVISTA survey. *Astrophys. J.* **777**, 18 (2013).

294. Weigel, A. K., Schawinski, K. & Bruderer, S. Stellar mass functions: methods, systematics and results for the local universe. *Mon. Not. R. Astron. Soc.* **459**, 2150–2187 (2016).

295. Dekel, A. & Silk, J. The origin of dwarf galaxies, cold dark matter, and biased galaxy formation. *Astrophys. J.* **303**, 39 (1986).

296. Larson, R. B. Effects of supernovae on the early evolution of galaxies. *Mon. Not. R. Astron. Soc.* **169**, 229–246 (1974).

297. White, S. D. M. & Frenk, C. S. Galaxy formation through hierarchical clustering. *Astrophys. J.* **379**, 52 (1991).

298. Pillepich, A. et al. First results from the IllustrisTNG simulations: the stellar mass content of groups and clusters of galaxies. *Mon. Not. R. Astron. Soc.* **475**, 648–675 (2018).

299. Werk, J. K. et al. The COS-Halos survey: physical conditions and baryonic mass in the low-redshift circumgalactic medium. *Astrophys. J.* **792**, 8 (2014).

300. Werk, J. K. et al. The COS-Halos survey: origins of the highly ionized circumgalactic medium of star-forming galaxies. *Astrophys. J.* **833**, 54 (2016).

301. Stern, J., Hennawi, J. F., Prochaska, J. X. & Werk, J. K. A universal density structure for circumgalactic gas. *Astrophys. J.* **830**, 87 (2016).

302. Rubin, K. H. R., Diamond-Stanic, A. M., Coil, A. L., Crofton, N. H. M. & Stewart, K. R. Galaxies probing galaxies in PRIMUS. II. The coherence scale of the cool circumgalactic medium. *Astrophys. J.* **868**, 142 (2018).

303. van de Voort, F., Springel, V., Mandelker, N., van den Bosch, F. C. & Pakmor, R. Cosmological simulations of the circumgalactic medium with 1 kpc resolution: enhanced H α column densities. *Mon. Not. R. Astron. Soc.* **482**, L85–L89 (2019).

304. Suresh, J., Nelson, D., Genel, S., Rubin, K. H. R. & Hernquist, L. Zooming in on accretion — II. Cold circumgalactic gas simulated with a super-Lagrangian refinement scheme. *Mon. Not. R. Astron. Soc.* **483**, 4040–4059 (2019).

305. Peeples, M. S. et al. Figuring out Gas & Galaxies in Enzo (FOGGIE). I. Resolving simulated circumgalactic absorption at $2 \leq z \leq 2.5$. *Astrophys. J.* **873**, 129 (2019).

306. Rasia, E. et al. Cool core clusters from cosmological simulations. *Astrophys. J. Lett.* **813**, L17 (2015).

307. Planelles, S. et al. On the role of AGN feedback on the thermal and chemodynamical properties of the hot intracluster medium. *Mon. Not. R. Astron. Soc.* **438**, 195–216 (2014).

308. Biffi, V. et al. On the nature of hydrostatic equilibrium in galaxy clusters. *Astrophys. J.* **827**, 112 (2016).

309. Vogelsberger, M. et al. The uniformity and time-invariance of the intra-cluster metal distribution in galaxy clusters from the IllustrisTNG simulations. *Mon. Not. R. Astron. Soc.* **474**, 2073–2093 (2018).

310. Barnes, D. J. et al. A census of cool-core galaxy clusters in IllustrisTNG. *Mon. Not. R. Astron. Soc.* **481**, 1809–1831 (2018).

311. Meneux, B. et al. The VIMOS-VLT Deep Survey (VVDS). The dependence of clustering on galaxy stellar mass at $z \sim 1$. *Astron. Astrophys.* **478**, 299–310 (2008).

312. Foucaud, S. et al. Clustering properties of galaxies selected in stellar mass: breaking down the link between luminous and dark matter in massive galaxies from $z = 0$ to $z = 2$. *Mon. Not. R. Astron. Soc.* **406**, 147–164 (2010).

313. Wake, D. A. et al. Galaxy clustering in the NEWFIRM medium band survey: the relationship between stellar mass and dark matter halo mass at $1 < z < 2$. *Astrophys. J.* **728**, 46 (2011).

314. Artale, M. C. et al. Small-scale galaxy clustering in the eagle simulation. *Mon. Not. R. Astron. Soc.* **470**, 1771–1787 (2017).

315. Marulli, F. et al. The VIMOS Public Extragalactic Redshift Survey (VIPERS): Luminosity and stellar mass dependence of galaxy clustering at $0.5 < z < 1.1$. *Astron. Astrophys.* **557**, A17 (2013).

316. Shen, S. et al. The size distribution of galaxies in the Sloan Digital Sky Survey. *Mon. Not. R. Astron. Soc.* **343**, 978–994 (2003).

317. Kormendy, J. & Ho, L. C. Coevolution (or not) of supermassive black holes and host galaxies. *Annu. Rev. Astron. Astrophys.* **51**, 511–653 (2013).

318. Tremonti, C. A. et al. The origin of the mass–metallicity relation: insights from 53,000 star-forming galaxies in the Sloan Digital Sky Survey. *Astrophys. J.* **613**, 898–913 (2004).

319. Davé, R., Rafieferantsoa, M. H., Thompson, R. J. & Hopkins, P. F. MUFASA: galaxy star formation, gas, and metal properties across cosmic time. *Mon. Not. R. Astron. Soc.* **467**, 115–132 (2017).

320. De Rossi, M. E., Bower, R. G., Font, A. S., Schaye, J. & Theuns, T. Galaxy metallicity scaling relations in the EAGLE simulations. *Mon. Not. R. Astron. Soc.* **472**, 3354–3377 (2017).

321. Torrey, P. et al. The evolution of the mass–metallicity relation and its scatter in IllustrisTNG. *Mon. Not. R. Astron. Soc.* **484**, 5587–5607 (2019).

322. Torrey, P. et al. Similar star formation rate and metallicity variability time-scales drive the fundamental metallicity relation. *Mon. Not. R. Astron. Soc.* **477**, L16–L20 (2018).

323. Trayford, J. W. et al. Colours and luminosities of $z = 0.1$ galaxies in the EAGLE simulation. *Mon. Not. R. Astron. Soc.* **452**, 2879–2896 (2015).

324. Nelson, D. et al. First results from the IllustrisTNG simulations: the galaxy colour bimodality. *Mon. Not. R. Astron. Soc.* **475**, 624–647 (2018).

325. Fall, S. M. & Efstathiou, G. Formation and rotation of disc galaxies with haloes. *Mon. Not. R. Astron. Soc.* **193**, 189–206 (1980).

326. Mo, H. J., Mao, S. & White, S. D. M. The formation of galactic discs. *Mon. Not. R. Astron. Soc.* **295**, 319–336 (1998).

327. Scannapieco, C., White, S. D. M., Springel, V. & Tissera, P. B. The formation and survival of discs in a Λ CDM universe. *Mon. Not. R. Astron. Soc.* **396**, 696696–696708 (2009).

328. Balogh, M. L., Pearce, F. R., Bower, R. G. & Kay, S. T. Revisiting the cosmic cooling crisis. *Mon. Not. R. Astron. Soc.* **326**, 1228–1234 (2001).

329. Brook, C. B. et al. Hierarchical formation of bulgeless galaxies: why outflows have low angular momentum. *Mon. Not. R. Astron. Soc.* **415**, 1051–1060 (2011).

330. Okamoto, T., Eke, V. R., Frenk, C. S. & Jenkins, A. Effects of feedback on the morphology of galaxy discs. *Mon. Not. R. Astron. Soc.* **363**, 1299–1314 (2005).

331. Brooks, A. M. et al. Interpreting the evolution of the size–luminosity relation for disk galaxies from redshift 1 to the present. *Astrophys. J.* **728**, 51 (2011).

332. Guedes, J., Callegari, S., Madau, P. & Mayer, L. Forming realistic late-type spirals in a Λ CDM universe: the Eris simulation. *Astrophys. J.* **742**, 76 (2011).

333. Aumer, M., White, S. D. M., Naab, T. & Scannapieco, C. Towards a more realistic population of bright spiral galaxies in cosmological simulations. *Mon. Not. R. Astron. Soc.* **434**, 3142–3164 (2013).

334. Marinacci, F., Pakmor, R. & Springel, V. The formation of disc galaxies in high-resolution moving-mesh cosmological simulations. *Mon. Not. R. Astron. Soc.* **437**, 1750–1775 (2014).

335. Wetzel, A. R. et al. Reconciling dwarf galaxies with Λ CDM cosmology: simulating a realistic population of satellites around a milky way-mass galaxy. *Astrophys. J. Lett.* **827**, L23 (2016).

336. Pakmor, R., Marinacci, F. & Springel, V. Magnetic fields in cosmological simulations of disk galaxies. *Astrophys. J.* **783**, L20 (2014).

337. Beck, R. Magnetic fields in spiral galaxies. *Astron. Astrophysics Rev.* **24**, 4 (2015).

338. Rieder, M. & Teyssier, R. A small-scale dynamo in feedback-dominated galaxies as the origin of cosmic magnetic fields — I. The kinematic phase. *Mon. Not. R. Astron. Soc.* **457**, 1722–1738 (2016).

339. Rieder, M. & Teyssier, R. A small-scale dynamo in feedback-dominated galaxies — II. The saturation phase and the final magnetic configuration. *Mon. Not. R. Astron. Soc.* **471**, 2674–2686 (2017).

340. Rieder, M. & Teyssier, R. A small-scale dynamo in feedback-dominated galaxies — III. Cosmological simulations. *Mon. Not. R. Astron. Soc.* **472**, 4368–4373 (2017).

341. Naab, T. et al. The ATLAS^{3D} project — XXV. Two-dimensional kinematic analysis of simulated galaxies and the cosmological origin of fast and slow rotators. *Mon. Not. R. Astron. Soc.* **444**, 3357–3387 (2014).

342. Kobayashi, C. GRAPE-SPH chemodynamical simulation of elliptical galaxies — II. Scaling relations and the fundamental plane. *Mon. Not. R. Astron. Soc.* **361**, 1216–1226 (2005).

343. Feldmann, R., Carollo, C. M. & Mayer, L. The Hubble sequence in groups: the birth of the early-type galaxies. *Astrophys. J.* **736**, 88 (2011).

344. Kobayashi, C. GRAPE-SPH chemodynamical simulation of elliptical galaxies — I. Evolution of metallicity gradients. *Mon. Not. R. Astron. Soc.* **347**, 740–758 (2004).

345. Oser, L., Ostriker, J. P., Naab, T., Johansson, P. H. & Burkert, A. The two phases of galaxy formation. *Astrophys. J. Lett.* **725**, 2312–2323 (2010).

346. Huang, S., Ho, L. C., Peng, C. Y., Li, Z.-Y. & Barth, A. J. Fossil evidence for the two-phase formation of elliptical galaxies. *Astrophys. J. Lett.* **768**, L28 (2013).

347. Rodriguez-Gomez, V. et al. The stellar mass assembly of galaxies in the Illustris simulation: growth by mergers and the spatial distribution of accreted stars. *Mon. Not. R. Astron. Soc.* **458**, 2371–2390 (2016).

348. Clauwens, B., Schaye, J., Franx, M. & Bower, R. G. The three phases of galaxy formation. *Mon. Not. R. Astron. Soc.* **478**, 3994–4009 (2018).

349. Lagos, C. D. P. et al. The connection between mass, environment, and slow rotation in simulated galaxies. *Mon. Not. R. Astron. Soc.* **476**, 4327–4345 (2018).

350. Schulze, F. et al. Kinematics of simulated galaxies — I. Connecting dynamical and morphological properties of early-type galaxies at different redshifts. *Mon. Not. R. Astron. Soc.* **480**, 4636–4658 (2018).

351. Green, A. M., Hofmann, S. & Schwarz, D. J. The power spectrum of SUSY-CDM on subgalactic scales. *Mon. Not. R. Astron. Soc.* **353**, L23–L27 (2004).

352. Bode, P., Ostriker, J. P. & Turok, N. Halo formation in warm dark matter models. *Astrophys. J.* **556**, 93–107 (2001).

353. Carlson, E. D., Machacek, M. E. & Hall, L. J. Self-interacting dark matter. *Astrophys. J.* **398**, 43–52 (1992).

354. Spergel, D. N. & Steinhardt, P. J. Observational evidence for self-interacting cold dark matter. *Phys. Rev. Lett.* **84**, 3760–3763 (2000).

355. Vogelsberger, M., Sijacki, D., Kereš, D., Springel, V. & Hernquist, L. Moving mesh cosmology: numerical techniques and global statistics. *Mon. Not. R. Astron. Soc.* **425**, 3024–3057 (2012).

356. Cyr-Racine, F.-Y. et al. ETHOS — an effective theory of structure formation: from dark particle physics to the matter distribution of the Universe. *Phys. Rev. D* **93**, 123527 (2016).

357. Vogelsberger, M. et al. ETHOS — an effective theory of structure formation: dark matter physics as a possible explanation of the small-scale CDM problems. *Mon. Not. R. Astron. Soc.* **460**, 1399–1416 (2016).

358. Vogelsberger, M., Zavala, J. & Loeb, A. Subhaloes in self-interacting galactic dark matter haloes. *Mon. Not. R. Astron. Soc.* **423**, 3740–3752 (2012).

359. Peter, A. H. G., Rocha, M., Bullock, J. S. & Kaplinghat, M. Cosmological simulations with self-interacting dark matter — II. Halo shapes versus observations. *Mon. Not. R. Astron. Soc.* **430**, 105–120 (2013).

360. Fry, A. B. et al. All about baryons: revisiting SIDM predictions at small halo masses. *Mon. Not. R. Astron. Soc.* **452**, 1468–1479 (2015).

361. Elbert, O. D. et al. Core formation in dwarf haloes with self-interacting dark matter: no fine-tuning necessary. *Mon. Not. R. Astron. Soc.* **453**, 29–37 (2015).

362. Hui, L., Ostriker, J. P., Tremaine, S. & Witten, E. Ultralight scalars as cosmological dark matter. *Phys. Rev. D* **95**, 043541 (2017).

363. Lee, J.-W. & Koh, I.-G. Galactic halos as boson stars. *Phys. Rev. D* **53**, 2236–2239 (1996).

364. Hu, W., Barkana, R. & Gruzinov, A. Fuzzy cold dark matter: the wave properties of ultralight particles. *Phys. Rev. Lett.* **85**, 1158–1161 (2000).

365. Peebles, P. J. E. Fluid dark matter. *Astrophys. J. Lett.* **534**, L127–L129 (2000).

366. Chavanis, P.-H. Mass-radius relation of Newtonian self-gravitating Bose–Einstein condensates with short-range interactions. I. Analytical results. *Phys. Rev. D* **84**, 043531 (2011).

367. Suárez, A., Robles, V. H. & Matos, T. in *Accelerated Cosmic Expansion: Astrophysics and Space Science Proceedings* Vol. 38 (eds Moreno González, C. et al.) 107 (Springer, 2014).

368. Matos, T., Vázquez-González, A. & Magaña, J. Phi squared as dark matter. *Mon. Not. R. Astron. Soc.* **393**, 1359–1369 (2009).

369. Lundgren, A. P., Bondarescu, M., Bondarescu, R. & Balakrishna, J. Lukewarm dark matter: Bose condensation of ultralight particles. *Astrophys. J. Lett.* **715**, L35–L39 (2010).

370. Robles, V. H. & Matos, T. Exact solution to finite temperature sfdm: natural cores without feedback. *Astrophys. J.* **763**, 19 (2013).

371. Seidel, E. & Suen, W.-M. Dynamical evolution of boson stars: perturbing the ground state. *Phys. Rev. D* **42**, 384–403 (1990).

372. Sin, S.-J. Late-time phase transition and the galactic halo as a Bose liquid. *Phys. Rev. D* **50**, 3650–3654 (1994).

373. Mocz, P. & Succi, S. Numerical solution of the nonlinear Schrödinger equation using smoothed-particle hydrodynamics. *Phys. Rev. D* **91**, 053304 (2015).

374. Nori, M. & Baldi, M. AX-GADGET: a new code for cosmological simulations of Fuzzy Dark Matter and Axion models. *Mon. Not. R. Astron. Soc.* **478**, 3935–3951 (2018).

375. Copeland, E. J., Sami, M. & Tsujikawa, S. Dynamics of dark energy. *Int. J. Mod. Phys. D* **15**, 1753–1935 (2006).

376. Baldi, M. Dark energy simulations. *Phys. Dark Universe* **1**, 162–193 (2012).

377. Linder, E. V. & Jenkins, A. Cosmic structure growth and dark energy. *Mon. Not. R. Astron. Soc.* **346**, 573–583 (2003).

378. Grossi, M. & Springel, V. The impact of early dark energy on non-linear structure formation. *Mon. Not. R. Astron. Soc.* **394**, 1559–1574 (2009).

379. Penzo, C., Macciò, A. V., Casarini, L., Stinson, G. S. & Wadsley, J. Dark MaGICC: the effect of dark energy on disc galaxy formation. Cosmology does matter. *Mon. Not. R. Astron. Soc.* **442**, 176–186 (2014).

380. Sefusatti, E. & Vernizzi, F. Cosmological structure formation with clustering quintessence. *J. Cosmol. Astropart. Phys.* **2011**, 047 (2011).

381. Amendola, L. & Tocchini-Valentini, D. Stationary dark energy: the present universe as a global attractor. *Phys. Rev. D* **64**, 043509 (2001).

382. Macciò, A. V., Quercellini, C., Mainini, R., Amendola, L. & Bonometto, S. A. Coupled dark energy: parameter constraints from N-body simulations. *Phys. Rev. D* **69**, 123516 (2004).

383. Baldi, M., Pettorino, V., Robbers, G. & Springel, V. Hydrodynamical N-body simulations of coupled dark energy cosmologies. *Mon. Not. R. Astron. Soc.* **403**, 1684–1702 (2010).

384. Li, B. & Barrow, J. D. N-body simulations for coupled scalar-field cosmology. *Phys. Rev. D* **83**, 024007 (2011).

385. Li, B. & Barrow, J. D. On the effects of coupled scalar fields on structure formation. *Mon. Not. R. Astron. Soc.* **413**, 262–270 (2011).

386. Milgrom, M. A modification of the Newtonian dynamics as a possible alternative to the hidden mass hypothesis. *Astrophys. J.* **270**, 365–370 (1983).

387. Famaey, B. & McGaugh, S. S. Modified Newtonian dynamics (MOND): observational phenomenology and relativistic extensions. *Living Rev. Relativ.* **15**, 10 (2012).

388. Bekenstein, J. D. Relativistic gravitation theory for the modified Newtonian dynamics paradigm. *Phys. Rev. D* **70**, 083509 (2004).

389. Skordis, C. Generalizing tensor-vector-scalar cosmology. *Phys. Rev. D* **77**, 123502 (2008).

390. McGaugh, S. S., Lelli, F. & Schombert, J. M. Radial acceleration relation in rotationally supported galaxies. *Phys. Rev. Lett.* **117**, 201101 (2016).

391. Lelli, F., McGaugh, S. S., Schombert, J. M. & Pawłowski, M. S. One law to rule them all: the radial acceleration relation of galaxies. *Astrophys. J.* **836**, 152 (2017).

392. Keller, B. W. & Wadsley, J. W. Λ CDM is consistent with SPARC radial acceleration relation. *Astrophys. J.* **835**, L17 (2017).

393. Ludlow, A. D. et al. Mass-discrepancy acceleration relation: a natural outcome of galaxy formation in cold dark matter halos. *Phys. Rev. Lett.* **118**, 161103 (2017).

394. Dutton, A. A., Macciò, A. V., Obreja, A. & Buck, T. NIHAO — XVIII. Origin of the MOND phenomenology of galactic rotation curves in a Λ CDM universe. *Mon. Not. R. Astron. Soc.* **485**, 1886–1899 (2019).

395. Llinares, C. Simulation techniques for modified gravity. *Int. J. Mod. Phys. D* **27**, 1848003 (2018).

396. Li, B., Zhao, G.-B., Teyssier, R. & Koyama, K. ECOSMOG: an efficient code for simulating modified gravity. *J. Cosmol. Astropart. Phys.* **1**, 051 (2012).

397. Puchwein, E., Baldi, M. & Springel, V. Modified-Gravity-GADGET: a new code for cosmological hydrodynamical simulations of modified gravity models. *Mon. Not. R. Astron. Soc.* **436**, 348–360 (2013).

398. Llinares, C., Mota, D. F. & Winther, H. A. ISIS: a new N -body cosmological code with scalar fields based on RAMSES. Code presentation and application to the shapes of clusters. *Astron. Astrophys.* **562**, A78 (2014).

399. Brax, P., Davis, A.-C., Li, B., Winther, H. A. & Zhao, G.-B. Systematic simulations of modified gravity: symmetron and dilaton models. *J. Cosmol. Astropart. Phys.* **2012**, 002 (2012).

400. Barreira, A., Li, B., Hellwing, W. A., Baugh, C. M. & Pascoli, S. Nonlinear structure formation in the cubic Galileon gravity model. *J. Cosmol. Astropart. Phys.* **2013**, 027 (2013).

401. Winther, H. A. et al. Modified gravity N -body code comparison project. *Mon. Not. R. Astron. Soc.* **454**, 4208–4234 (2015).

402. Fontanot, F., Puchwein, E., Springel, V. & Bianchi, D. Semi-analytic galaxy formation in $f(R)$ -gravity cosmologies. *Mon. Not. R. Astron. Soc.* **436**, 2672–2679 (2013).

403. Jennings, E., Baugh, C. M., Li, B., Zhao, G.-B. & Koyama, K. Redshift-space distortions in $f(R)$ gravity. *Mon. Not. R. Astron. Soc.* **425**, 2128–2143 (2012).

404. Naik, A. P., Puchwein, E., Davis, A.-C. & Arnold, C. Imprints of chameleon $f(R)$ gravity on galaxy rotation curves. *Mon. Not. R. Astron. Soc.* **480**, 5211–5225 (2018).

405. Lombriser, L. & Peñarrubia, J. How chameleons core down cusps. *Phys. Rev. D* **91**, 084022 (2015).

406. Arnold, C., Leo, M. & Li, B. Realistic simulations of galaxy formation in $f(R)$ modified gravity. *Nat. Astron.* **3**, 945–954 (2019).

407. Davis, A.-C., Lim, E. A., Sakstein, J. & Shaw, D. J. Modified gravity makes galaxies brighter. *Phys. Rev. D* **85**, 123006 (2012).

408. Stadel, J. et al. Quantifying the heart of darkness with GHALO — a multibillion particle simulation of a galactic halo. *Mon. Not. R. Astron. Soc.* **398**, L21–L25 (2009).

409. Garrison-Kimmel, S., Boylan-Kolchin, M., Bullock, J. S. & Lee, K. ELVIS: exploring the local volume in simulations. *Mon. Not. R. Astron. Soc.* **438**, 2578–2596 (2014).

410. Dolag, K. The magneticum simulations, from galaxies to galaxy clusters. *IAU Highl. Astron.* **29**, 2250156 (2015).

411. Khandai, N. et al. The massiveblack-II simulation: the evolution of haloes and galaxies to $z \sim 0$. *Mon. Not. R. Astron. Soc.* **450**, 1349–1374 (2015).

412. Teyssier, R. Cosmological hydrodynamics with adaptive mesh refinement. A new high resolution code called RAMSES. *Astron. Astrophys.* **385**, 337–364 (2002).

413. Springel, V. The cosmological simulation code GADGET-2. *Mon. Not. R. Astron. Soc.* **364**, 1105–1134 (2005).

414. Bryan, G. L. et al. ENZO: an adaptive mesh refinement code for astrophysics. *Astrophys. J. Suppl.* **211**, 19 (2014).

415. Jetley, P., Kale, L. V., Gioachin, F., Quinn, T. & Mendes, C. Massively parallel cosmological simulations with change. In *2008 IEEE International Parallel & Distributed Processing Symposium 1–12*; <https://doi.ieeecomputersociety.org/10.1109/IPDPS.2008.4536319> (IEEE Computer Society, 2008).

416. Gioachin, F., Kalé, L. V., Quinn, T. R., Jetley, P. & Wesolowski, L. Scaling hierarchical N -body simulations on GPU clusters. In *SC Conference 1–11*; <https://doi.ieeecomputersociety.org/10.1109/SC.2010.49> (IEEE Computer Society, 2010).

417. Menon, H. et al. Adaptive techniques for clustered N -body cosmological simulations. *Comput. Astrophys. Cosmol.* **2**, 1 (2015).

418. Habib, S. et al. HACC: simulating sky surveys on state-of-the-art supercomputing architectures. *New Astron.* **42**, 49–65 (2016).

419. Potter, D., Stadel, J. & Teyssier, R. PKDGRAV3: beyond trillion particle cosmological simulations for the next era of galaxy surveys. *Comput. Astrophys. Cosmol.* **4**, 2 (2017).

420. Wadsley, J. W., Keller, B. W. & Quinn, T. R. Gasoline2: a modern smoothed particle hydrodynamics code. *Mon. Not. R. Astron. Soc.* **471**, 2357–2369 (2017).

421. Schaller, M., Gonnet, P., Chalk, A. B. G. & Draper, P. W. SWIFT: SPH with inter-dependent fine-grained tasking. *GitHub* <https://github.com/SWIFTSIM/swiftsim> (2018).

422. Springel, V. et al. Simulations of the formation, evolution and clustering of galaxies and quasars. *Nature* **435**, 629–636 (2005).

423. Boylan-Kolchin, M., Springel, V., White, S. D. M., Jenkins, A. & Lemson, G. Resolving cosmic structure formation with the Millennium-II simulation. *Mon. Not. R. Astron. Soc.* **398**, 1150–1164 (2009).

424. Teyssier, R. et al. Full-sky weak-lensing simulation with 70 billion particles. *Astron. Astrophys.* **497**, 335–341 (2009).

425. Klypin, A. A., Trujillo-Gomez, S. & Primack, J. Dark matter halos in the standard cosmological model: results from the bolshoi simulation. *Astrophys. J.* **740**, 102 (2011).

426. Alimi, J.-M. et al. DEUS full observable Λ CDM universe simulation: the numerical challenge. Preprint at [arXiv https://arxiv.org/abs/1206.2838](https://arxiv.org/abs/1206.2838) (2012).

427. Prada, F., Klypin, A. A., Cuesta, A. J., Betancort-Rijo, J. E. & Primack, J. Halo concentrations in the standard Λ cold dark matter cosmology. *Mon. Not. R. Astron. Soc.* **423**, 3018–3030 (2012).

428. Ishiyama, T. et al. The v^2 GC simulations: quantifying the dark side of the universe in the Planck cosmology. *Publ. Astron. Soc. Jpn.* **67**, 61 (2015).

429. Diemand, J. et al. Clumps and streams in the local dark matter distribution. *Nature* **454**, 735–738 (2008).

430. Libeskind, N. I. et al. Constrained simulations of the local group: on the radial distribution of substructures. *Mon. Not. R. Astron. Soc.* **401**, 1889–1897 (2010).

431. Hellwing, W. A. et al. The Copernicus Complexio: a high-resolution view of the small-scale Universe. *Mon. Not. R. Astron. Soc.* **457**, 3492–3505 (2016).

432. Dubois, Y. et al. Dancing in the dark: galactic properties trace spin swings along the cosmic web. *Mon. Not. R. Astron. Soc.* **444**, 1453–1468 (2014).

433. Feng, Y. et al. The BlueTides simulation: first galaxies and reionization. *Mon. Not. R. Astron. Soc.* **455**, 2778–2791 (2016).

434. Davé, R., Thompson, R. & Hopkins, P. F. MUFASA: galaxy formation simulations with meshless hydrodynamics. *Mon. Not. R. Astron. Soc.* **462**, 3265–3284 (2016).

435. McCarthy, I. G., Schaye, J., Bird, S. & Le Brun, A. M. C. The BAHAMAS project: calibrated hydrodynamical simulations for large-scale structure cosmology. *Mon. Not. R. Astron. Soc.* **465**, 2936–2965 (2017).

436. Tremmel, M. et al. The ROMULUS cosmological simulations: a physical approach to the formation, dynamics and accretion models of SMBHs. *Mon. Not. R. Astron. Soc.* **470**, 1121–1139 (2017).

437. Sawala, T. et al. The APOSTLE simulations: solutions to the Local Group's cosmic puzzles. *Mon. Not. R. Astron. Soc.* **457**, 1931–1943 (2016).

438. Barnes, D. J. et al. The redshift evolution of massive galaxy clusters in the MACSIS simulations. *Mon. Not. R. Astron. Soc.* **465**, 213–233 (2017).

439. Cui, W. et al. The three hundred project: a large catalogue of theoretically modelled galaxy clusters for cosmological and astrophysical applications. *Mon. Not. R. Astron. Soc.* **480**, 2898–2915 (2018).

440. Henden, N. A., Puchwein, E., Shen, S. & Sijacki, D. The FABLE simulations: a feedback model for galaxies, groups, and clusters. *Mon. Not. R. Astron. Soc.* **479**, 5385–5412 (2018).

441. Tremmel, M. et al. Introducing ROMULUSC: a cosmological simulation of a galaxy cluster with an unprecedented resolution. *Mon. Not. R. Astron. Soc.* **483**, 3336–3362 (2019).

442. Kauffmann, G., White, S. D. M. & Guiderdoni, B. The formation and evolution of galaxies within merging dark matter haloes. *Mon. Not. R. Astron. Soc.* **264**, 201–218 (1993).

443. Somerville, R. S. & Primack, J. R. Semi-analytic modelling of galaxy formation: the local Universe. *Mon. Not. R. Astron. Soc.* **310**, 1087–1110 (1999).

444. Bower, R. G. et al. Breaking the hierarchy of galaxy formation. *Mon. Not. R. Astron. Soc.* **370**, 645–655 (2006).

445. Croton, D. J. et al. The many lives of active galactic nuclei: cooling flows, black holes and the luminosities and colours of galaxies. *Mon. Not. R. Astron. Soc.* **365**, 11–28 (2006).

446. Guo, Q. et al. From dwarf spheroidals to cD galaxies: simulating the galaxy population in a Λ CDM cosmology. *Mon. Not. R. Astron. Soc.* **413**, 101–131 (2011).

447. Bullock, J. S. & Boylan-Kolchin, M. Small-scale challenges to the Λ CDM paradigm. *Annu. Rev. Astron. Astrophys.* **55**, 343–387 (2017).

448. Klypin, A., Kravtsov, A. V., Valenzuela, O. & Prada, F. Where are the missing galactic satellites? *Astrophys. J.* **522**, 82–92 (1999).

449. Zavala, J. et al. The velocity function in the local environment from Λ CDM and Λ WDM constrained simulations. *Astrophys. J.* **700**, 1779–1793 (2009).

450. Papastergis, E., Martin, A. M., Giovanelli, R. & Haynes, M. P. The velocity width function of galaxies from the 40% ALFALFA survey: shedding light on the cold dark matter overabundance problem. *Astrophys. J.* **739**, 38 (2011).

451. Klypin, A., Karachentsev, I., Makarov, D. & Nasonova, O. Abundance of field galaxies. *Mon. Not. R. Astron. Soc.* **454**, 1798–1810 (2015).

452. de Blok, W. J. G. & McGaugh, S. S. The dark and visible matter content of low surface brightness disc galaxies. *Mon. Not. R. Astron. Soc.* **290**, 533–552 (1997).

453. Walker, M. G. & Peñarrubia, J. A method for measuring (slopes of) the mass profiles of dwarf spheroidal galaxies. *Astrophys. J.* **742**, 20 (2011).

454. Boylan-Kolchin, M., Bullock, J. S. & Kaplinghat, M. Too big to fail? The puzzling darkness of massive Milky Way subhaloes. *Mon. Not. R. Astron. Soc.* **415**, L40–L44 (2011).

455. Papastergis, E., Giovanelli, R., Haynes, M. P. & Shankar, F. Is there a ‘too big to fail’ problem in the field? *Astron. Astrophys.* **574**, A113 (2015).

456. Oman, K. A. et al. The unexpected diversity of dwarf galaxy rotation curves. *Mon. Not. R. Astron. Soc.* **452**, 3650–3665 (2015).

457. Navarro, J. F., Eke, V. R. & Frenk, C. S. The cores of dwarf galaxy haloes. *Mon. Not. R. Astron. Soc.* **283**, L72–L78 (1996).

458. Governato, F. et al. Cuspy no more: how outflows affect the central dark matter and baryon distribution in Λ cold dark matter galaxies. *Mon. Not. R. Astron. Soc.* **422**, 1231–1240 (2012).

459. Oñorbe, J. et al. Forged in FIRE: cusps, cores and baryons in low-mass dwarf galaxies. *Mon. Not. R. Astron. Soc.* **454**, 2092–2106 (2015).

460. Chan, T. K. et al. The impact of baryonic physics on the structure of dark matter haloes: the view from the FIRE cosmological simulations. *Mon. Not. R. Astron. Soc.* **454**, 2981–3001 (2015).

461. Read, J. I., Agertz, O. & Collins, M. L. M. Dark matter cores all the way down. *Mon. Not. R. Astron. Soc.* **459**, 2573–2590 (2016).

Acknowledgements

The authors thank D. Barnes, M. Boylan-Kolchin, L. Hernquist, R. Kannan, H. Li, S. O’Neil, R. Pakmor, C. Pfrommer, L. Sales, A. Smith, V. Springel and R. Weinberger for useful comments. The authors also thank the reviewers for helpful feedback. M.V. acknowledges support through a Massachusetts Institute of Technology (MIT) RSC award, a Kavli Research Investment Fund, NASA ATP grant NNX17AG29G and National Science Foundation (NSF) grants AST-1814053 and AST-1814259. F.M. acknowledges support through the programme ‘Rita Levi Montalcini’ of the Italian Ministry of Education, University and Research.

Author contributions

The authors contributed equally to all aspects of the article.

Competing interests

The authors declare no competing interests.

Peer review information

Nature Reviews Physics thanks Jeremiah Ostriker, Matthieu Schaller and Naoki Yoshida for their contribution to the peer review of this work.

Publisher’s note

Springer Nature remains neutral with regard to jurisdictional claims in published maps and institutional affiliations.